Electronic Supplementary Information

The anticancer activity of an air-stable Pd(I)-NHC (NHC = N-heterocyclic carbene) dimer

Thomas Scattolin, Enrica Bortolamiol, Stefano Palazzolo, Isabella Caligiuri, Tiziana Perin, Vincenzo Canzonieri, Nicola Demitri, Flavio Rizzolio,* Luigi Cavallo, Busra Dereli, Manoj V. Mane, Steven P. Nolan and Fabiano Visentin*

Table of Contents

General information

The palladium(II) precursors [Pd(μ-Cl)(1,1-dimethylallyl)]$_2$,[1] [Pd(MePy-CH_2SPh)(1,1-dimethylallyl)]ClO_4 **1**[2] and the silver compounds [Ag_2(Mes-Im-CH_2-Im-Mes)Br_2][3] and [Ag_2(Bn-Im-CH_2-Im-Bn)Br_2][3] were synthesized according to published procedures.

Solvents and all other reagents were purchased and used as received without further purification unless otherwise stated. ^{1}H and ^{13}C{^{1}H} Nuclear Magnetic Resonance (NMR) spectra were recorded on a Bruker Advance 400 spectrometer at 298K. Chemical shifts (expressed by parts per million) are referenced to residual solvent peaks.

IR were recorded on a Perkin-Elmer Spectrum One spectrophotometer.

Elemental analysis was carried out using an Elemental CHN "CUBO Micro Vario" analyzer.

Conductivity measurements were performed by Conductivity Radiometer Copenhagen CDM3.

ESI-MS analyses were performed using a LCQ-Duo (Thermo-Finnigan) operating in positive ion mode (capillary voltage 10 V, spray voltage 4.5 kV, capillary temperature 200 °C, mass scan range from 150 to 2000 amu).

UV-Vis spectra were recorded on a Lambda 40 UV/Vis spectrophotometer equipped with a Perkin-Elmer PTP 6 (Peltier temperature programmer) apparatus.

Synthesis of Pd(I) dimer 3

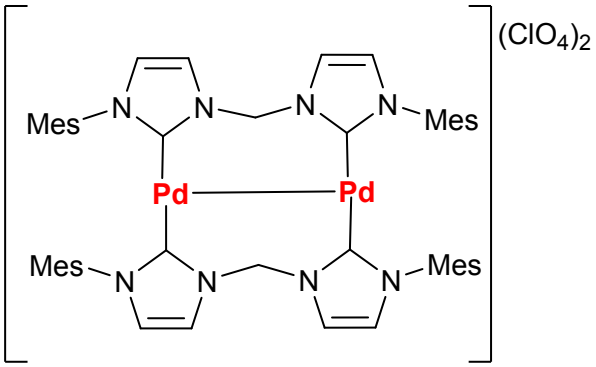

In a 50 mL round-bottom flask, 0.1603 g (0.3270 mmol) of the precursor[Pd(Me-PyCH$_2$SPh)(η^3-1,1-dimethylC$_3$H$_3$)]ClO$_4$ **1** was dissolved in 15 mL of dichloromethane. Subsequently, 0.2485 g (0.3270 mmol) of the silver complex [Ag$_2$(Mes-Im-CH$_2$-Im-Mes)Br$_2$], previously dissolved in ca. 5 mL of CH$_2$Cl$_2$, was added. The mixture was stirred at room temperature for 15 min and the precipitated AgBr was removed by filtration on a millipore membrane filter.

The solvent was removed under vacuum and them, the mixture of the Pd(II) allyl complex **2** and the Pd(I) dimer **3** was dissolved in a CH$_2$Cl$_2$/Et$_2$O mixture (30 mL : 70 mL) and set at 5°C overnight. After this time, the Pd(I) dimer **3** precipitated as a pink microcrystalline solid which was filtered and dried under vacuum.

0.0354 g of **3** was obtained (Yield: 22%).

^{1}H NMR (300 MHz, d^6-DMSO, T=298 K, ppm) δ: 1.26 (s, 12H, 4 o-aryl-CH$_3$), 1.59 (s, 12H, 4 o-aryl-CH$_3$), 2.43 (s, 12H, 4 p-aryl-CH$_3$), 6.51 and 7.23 (AB system, J= 13.6 Hz, 4H, 2NCH$_2$N), 6.95-7.07 (8H, Ar-H), 7.45-8.03 (8H, CH^{Im}).

^{13}C{^{1}H} NMR (d^6-DMSO, T=298 K, ppm) δ: 16.8 (CH$_3$, o-Mesityl-CH$_3$), 17.2 (CH$_3$, o-Mesityl-CH$_3$), 21.2 (CH$_3$, p-Mesityl-CH$_3$), 64.0 (CH$_2$, NCH$_2$N), 122.6-125.1 (CH, CH=CH^{Im}), 129.6-139.3 (Ar-C), 182.8 (C, carbene).

Anal. Calc. for C$_{50}$H$_{56}$Cl$_2$N$_8$O$_8$Pd$_2$: C, 50.86; H, 4.78; N, 9.49. Found: C, 51.02; H, 4.70; N, 9.57%.

IR [KBr Pellet]: ν_{ClO} = 1083 cm^{-1}, δ_{ClO} = 621 cm^{-1}.

Λ_M (DMSO, 10^{-3}M, 298 K): 46.0 ohm^{-1} cm^2 mol^{-1}

Synthesis of Pd(II) allyl complex 2

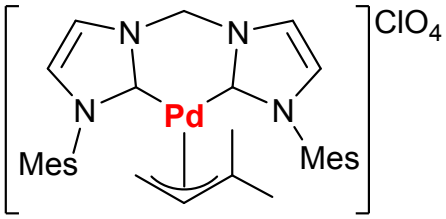

The CH_2Cl_2/Et_2O solution removed during the filtration of the Pd(I) dimer **3** was concentrated under vacuum and the brownish solid (compound **2**) was precipitated by addition of diethylether. 0.1224 g of **2** was obtained (Yield: 57%).

^{1}H NMR (300 MHz, $CDCl_3$, T=298 K, ppm) δ: 0.55 (s, 3H, allyl-CH_3), 1.27 (s, 3H, allyl-CH_3), 1.50 (d, J=12.0 Hz , 1H, *anti* allyl-H), 1.96 (s, 3H, o-aryl-CH_3), 1.99 (s, 6H, 2 o-aryl-CH_3), 2.04 (s, 3H, o-aryl-CH_3), 2.36 (s, 6H, 2 p-aryl-CH_3), 2.63 (d, J=6.4 Hz , 1H, *syn* allyl-H), 4.54 (m, H, *central* allyl-H), 6.22-6.76 (AB system, J= 11.6 Hz, 2H, NCH_2N), 6.80-8.05 (8H, Ar-H).

^{13}C{^{1}H} NMR ($CDCl_3$, T=298 K, ppm) δ: 17.8 (CH_3, o-Mesityl-CH_3), 18.0 (CH_3, o-Mesityl-CH_3), 18.2 (CH_3, o-Mesityl-CH_3), 18.3 (CH_3, o-Mesityl-CH_3), 19.7 (CH_3, allyl CH_3), 21.0 (CH_3, p-Mesityl-CH_3), 22.6 (CH_3, p-Mesityl-CH_3), 26.2 (CH_3, allyl CH_3), 46.6 (CH_2, allyl CH_2), 62.9 (CH_2, NCH_2N), 98.3 (C, allyl-C) 111.7 (CH, *central* allyl-CH), 122.2-123.3 (CH, $CH{=}CH^{Im}$), 128.9-139.5 (Ar-C), 177.0 (C, carbene), 179.0 (C, carbene).

Anal. Calc. for $C_{30}H_{37}ClN_4O_4Pd$: C, 54.64; H, 5.66; N, 8.50. Found: C, 54.76; H, 5.70; N, 8.39%.

IR [KBr Pellet]: ν_{ClO} = 1085 cm^{-1}, δ_{ClO} = 620 cm^{-1}.

Reactivity studies of Ag-bisNHC complexes with different Pd(II)-allyl complexes

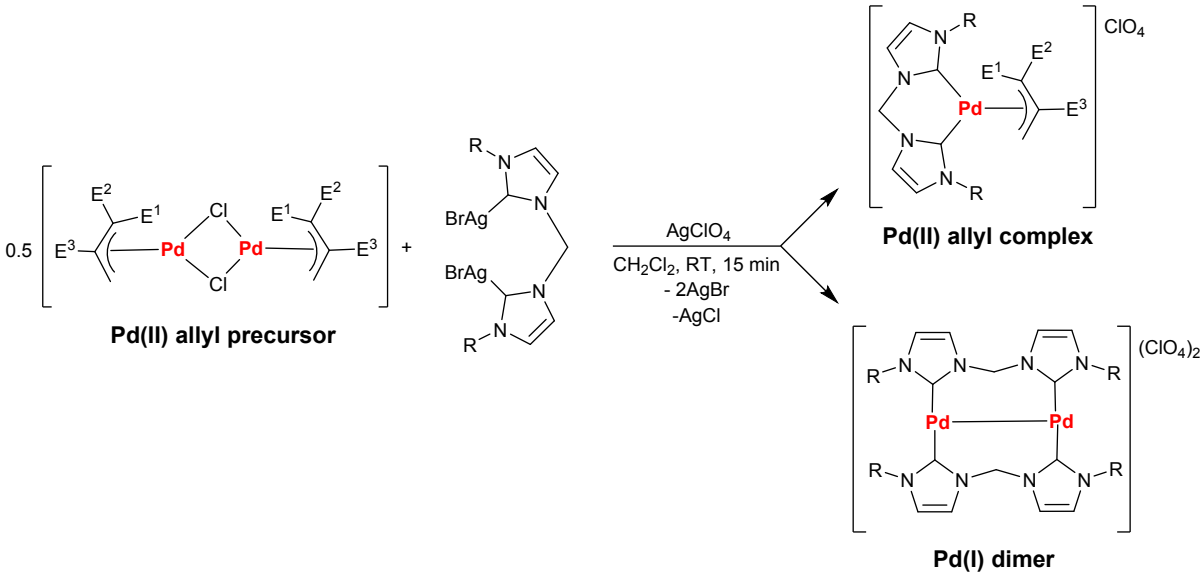

Table S1

Entry	E^1	E^2	E^3	R	% Pd(I) dimer
1	Me	Me	H	Mes	40
2	Me	Me	H	Bn	0
3	H	H	H	Mes	0
4	H	H	Me	Mes	0
5	Ph	H	H	Mes	10

Entry 1

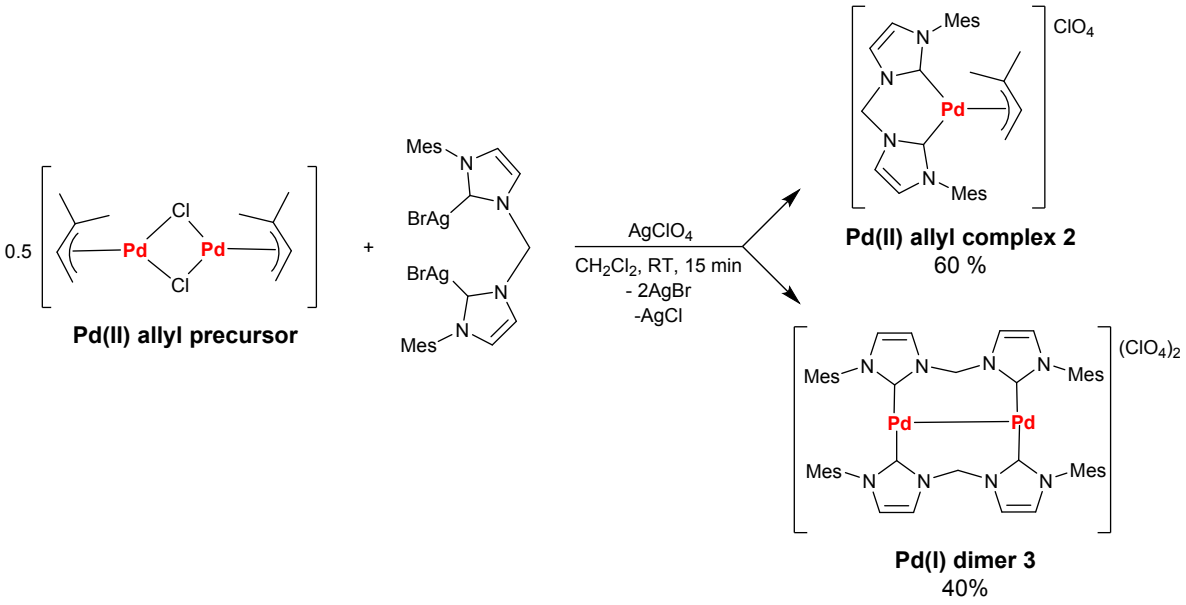

In a 2 mL vial 6.2 mg of the precursor $[Pd(\mu\text{-}Cl)(\eta^3\text{-}1,1\text{-dimethyl}C_3H_3)]_2$ (0.015 mmol) was dissolved in 0.6 mL of dichloromethane. Subsequently, 0.0223 g (0.029 mmol, 2 equiv.) of the silver complex $[Ag_2(Mes\text{-}Im\text{-}CH_2\text{-}Im\text{-}Mes)Br_2]$ and 6.1 mg of $AgClO_4$ (0.029 mmol, 2 equiv.) were added.

The mixture was stirred at room temperature for 15 min.

After this time the precipitated AgBr was removed by filtration on a millipore membrane filter and the solvent was removed in vacuo.

^1H NMR spectrum (see Fig. S8) reveals the presence of a 40:60 mixture of Pd(I) dimer **3** and palladium allyl complex **2**, as previously observed when $[Pd(Me\text{-}PyCH_2SPh)(\eta^3\text{-}1,1\text{-dimethyl}C_3H_3)]ClO_4$ **1** is used as palladium source (see Fig. S1).

Entry 2

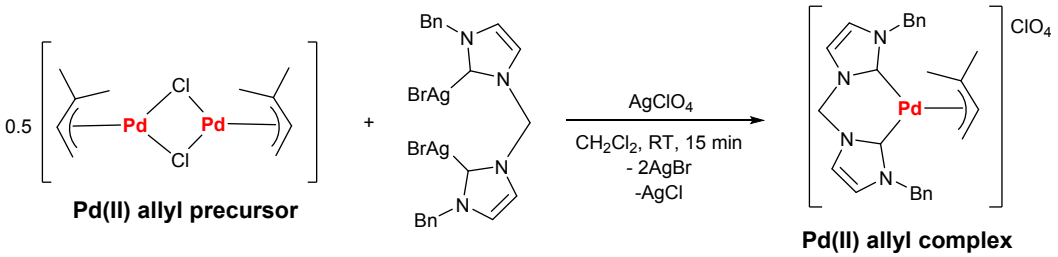

In a 2 mL vial 6.0 mg of the precursor $[Pd(\mu\text{-}Cl)(\eta^3\text{-}1,1\text{-dimethylC}_3H_3)]_2$ (0.014 mmol) was dissolved in 0.6 mL of dichloromethane. Subsequently, 0.0200 g (0.028 mmol, 2 equiv.) of the silver complex $[Ag_2(Bn\text{-}Im\text{-}CH_2\text{-}Im\text{-}Bn)Br_2]$ and 5.9 mg of $AgClO_4$ (0.028 mmol, 2 equiv.) were added.

The mixture was stirred at room temperature for 15 min and after this time the solvent was removed in vacuo.

^{1}H NMR spectrum (see Fig. S9) reveals the presence of a single set of signals which is consistent with a palladium allyl complex bearing the chelating bisNHC**.**

^{1}H NMR (300 MHz, $CDCl_3$, T=298 K, ppm) δ: 1.38 (s, 3H, allyl-CH_3), 1.61 (s, 3H, allyl-CH_3), 3.50 (d, J = 6.6 Hz , 1H, *syn* allyl-H), 5.05-5.28 (m, 5H, *central* allyl-H, $2CH_2Ph$), 6.79 (d, 1H, J = 1.0 Hz, $CH{=}CH^{Im}$), 6.89 (s, 1H, $CH{=}CH^{Im}$), 6.80-8.05 (12H, Ar-H, NHC_2N), 7.86 (s, 1H, $CH{=}CH^{Im}$), 7.89 (d, 1H, J = 1.0 Hz, $CH{=}CH^{Im}$).

Entry 3

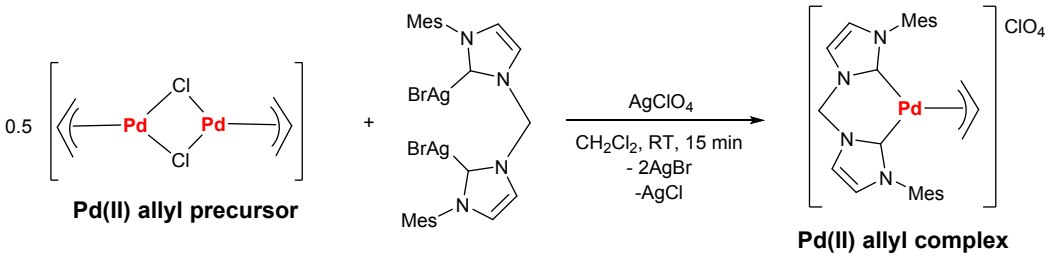

In a 2 mL vial 5.7 mg of the precursor $[Pd(\mu\text{-}Cl)(\eta^3\text{-}C_3H_5)]_2$ (0.016 mmol) was dissolved in 0.6 mL of dichloromethane. Subsequently, 0.0237 g (0.031 mmol, 2 equiv.) of the silver complex $[Ag_2(Mes\text{-}Im\text{-}CH_2\text{-}Im\text{-}Mes)Br_2]$ and 6.5 mg of $AgClO_4$ (0.031 mmol, 2 equiv.) were added.

The mixture was stirred at room temperature for 15 min and after this time the solvent was removed in vacuo.

^{1}H NMR spectrum (see Fig. S10) reveals the presence of two sets of signals which are consistent with the palladium allyl complex bearing the chelating bisNHC previously reported by our group.[4]

Major isomer (ca. 60%):

^{1}H NMR (300 MHz, $CDCl_3$, T = 298 K, ppm) δ: 1.87 (d, J = 13.8 Hz, 2H, 2 *anti* allyl-H), 1.91 (s, 6H, 2 o-mesityl-CH_3), 1.96 (s, 6H, 2 o-mesityl-CH_3), 2.35 (s, 6H, 2 p-mesityl-CH_3), 2.94 (d, J = 7.5 Hz, 2H, 2 *syn* allyl-H), 4.68 (m, 1H, *central* allyl-H), 6.33-6.84 (AB system, J = 13.2 Hz, 2H, NCH_2N), 6.85-8.16 (8H, Ar-H, 2CH=CH^{Im}).

Minor isomer (ca. 40%):

^{1}H NMR (300 MHz, $CDCl_3$, T = 298 K, ppm) δ: 1.37 (s, 6H, 2 o-mesityl-CH_3), 1.66 (s, 6H, 2 o-mesityl-CH_3), 1.68 (d, J = 13.6 Hz, 2H, 2 *anti* allyl-H), 2.36 (d, J = 7.4 Hz, 2H, 2 *syn* allyl-H), 2.47 (s, 6H, 2 p-mesityl-CH_3), 4.68 (m, 1H, *central* allyl-H) 6.33-6.84 (AB system, J = 13.7 Hz, 2H, NCH_2N), 6.85-8.16 (8H, Ar-H, 2CH=CH^{Im}).

Entry 4

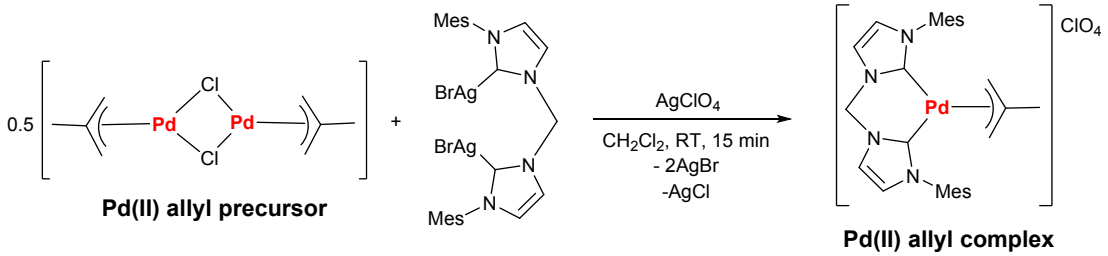

In a 2 mL vial 5.9 mg of the precursor $[Pd(\mu\text{-}Cl)(\eta^3\text{-}2\text{-methyl-}C_3H_4)]_2$ (0.015 mmol) was dissolved in 0.6 mL of dichloromethane. Subsequently, 0.0228 g (0.030 mmol, 2 equiv.) of the silver complex $[Ag_2(Mes\text{-}Im\text{-}CH_2\text{-}Im\text{-}Mes)Br_2]$ and 6.2 mg of $AgClO_4$ (0.030 mmol, 2 equiv.) were added.

The mixture was stirred at room temperature for 15 min and after this time the solvent was removed in vacuo.

^{1}H NMR spectrum (see Fig. S11) reveals the presence of two sets of signals which are consistent with two different atropoisomers of the palladium allyl complex bearing the chelating bisNHC previously reported by our group.[4]

Major isomer (ca. 52%):

^{1}H NMR (300 MHz, $CDCl_3$, T = 298 K, ppm) δ: 1.18 (s, 3H, allyl-CH_3), 1.80 (s, 2H, 2 *anti* allyl-H), 1.86 (s, 6H, 2 o-mesityl-CH_3), 1.97 (s, 6H, 2 o-mesityl-CH_3), 2.37 (s, 6H, 2 p-mesityl-CH_3), 2.52 (s, 2H, 2 *syn* allyl-H), 6.51-6.73 (AB system, J= 13.2 Hz, 2H, NCH_2N), 6.85-8.15 (8H, Ar-H, 2CH=CH^{Im}).

Minor isomer (ca. 48%):

^{1}H NMR (300 MHz, $CDCl_3$, T = 298 K, ppm) δ: 1.37 (s, 6H, 2 o-mesityl-CH_3), 1.51 (s, 3H, allyl-CH_3), 1.67 (s, 6H, 2 o-mesityl-CH_3), 1.81 (s, 2H, 2 *anti* allyl-H), 2.39 (s, 2H, 2 *syn* allyl-H), 2.47 (s, 6H, 2 p-mesityl-CH_3), 6.86-6.96 (AB system, J = 13.6 Hz, 2H, NCH_2N), 6.85-8.15 (8H, Ar-H, 2CH=CH^{Im}).

Entry 5

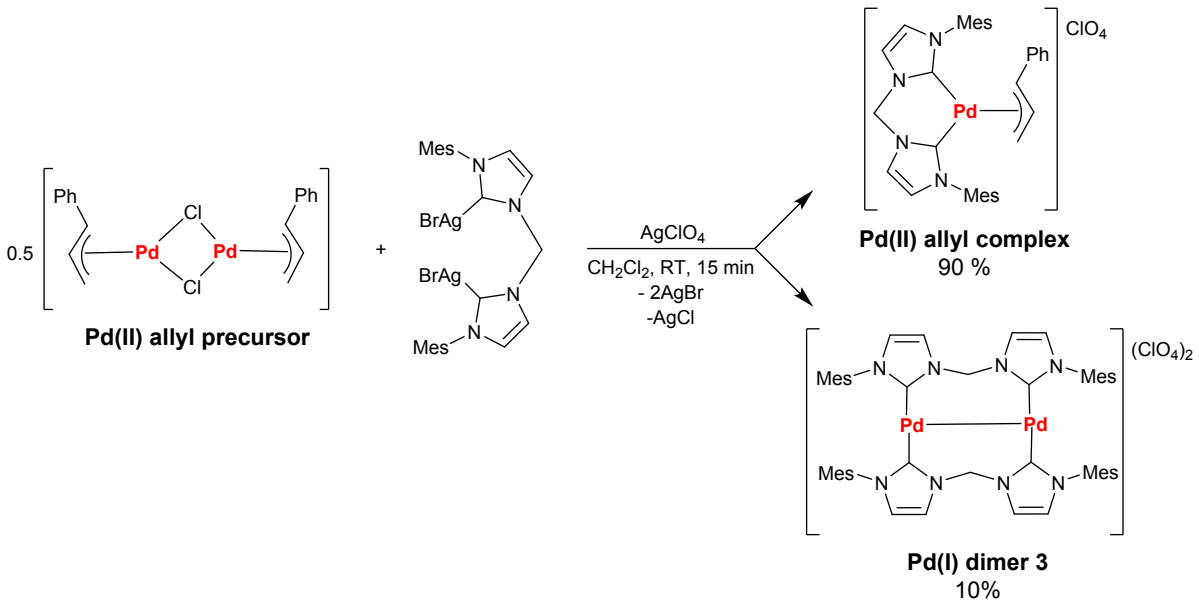

In a 2 mL vial 6.7 mg of the precursor $[Pd(\mu\text{-}Cl)(\eta^3\text{-}1\text{-phenyl-}C_3H_4)]_2$ (0.013 mmol) was dissolved in 0.6 mL of dichloromethane. Subsequently, 0.0196 g (0.026 mmol, 2 equiv.) of the silver complex $[Ag_2(Mes\text{-}Im\text{-}CH_2\text{-}Im\text{-}Mes)Br_2]$ and 5.4 mg of $AgClO_4$ (0.026 mmol, 2 equiv.) were added.

The mixture was stirred at room temperature for 15 min.

After this time the precipitated AgBr was removed by filtration on a millipore membrane filter and the solvent was removed in vacuo.

^1H NMR spectrum (see Fig. S12) reveals the presence of a 10:90 mixture of Pd(I) dimer **3** and corresponding palladium allyl complex.

NMR, UV-Vis and ESI-MS spectra

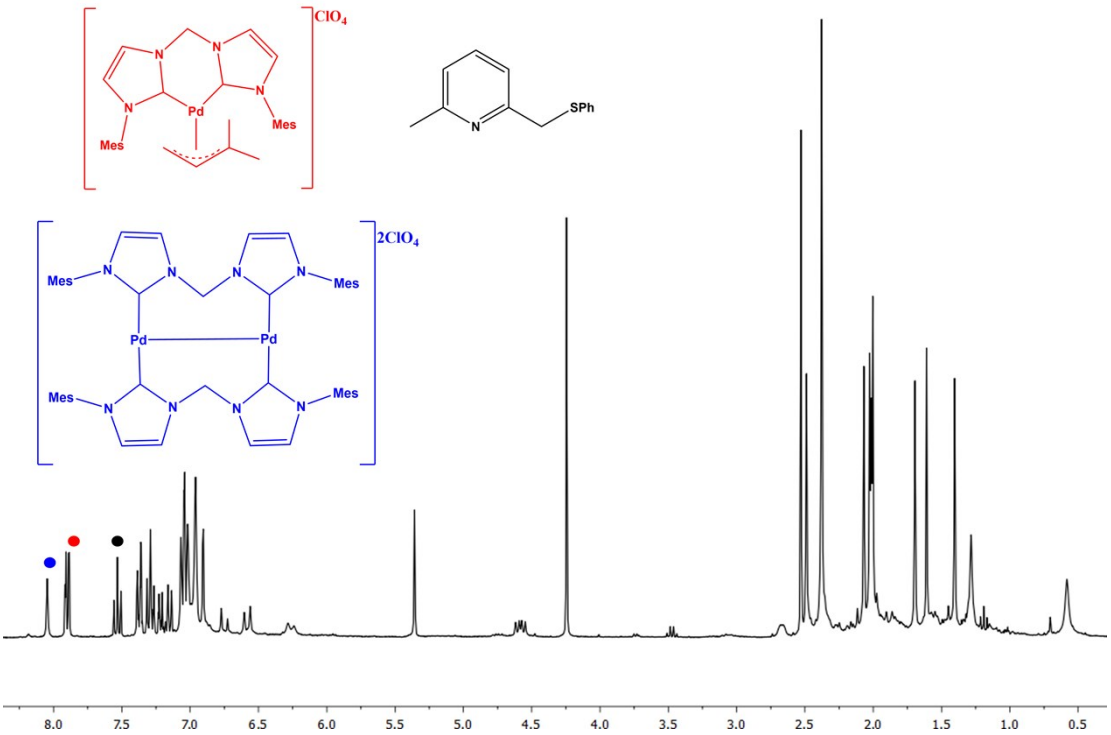

Figure S1: ^{1}H NMR spectrum in CD_2Cl_2 at RT for the reaction: **1** + [Ag_2(Mes-Im-CH_2-Im-Mes)Br_2] –> Pd(II)-(1,1-dimethyl-allyl) complex **2** + Pd(I) dimer **3** + 2-methyl-6-(phenylthiomethyl)pyridine

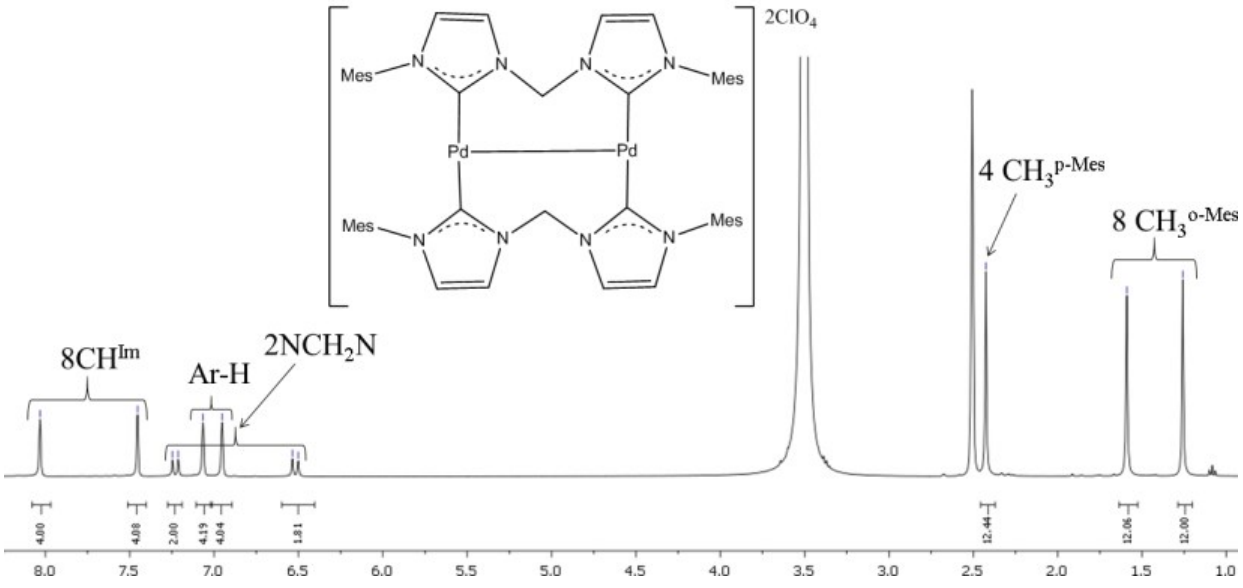

Figure S2: ^{1}H NMR spectrum of Pd(I) dimer **3** in DMSO-d6 at 298 K

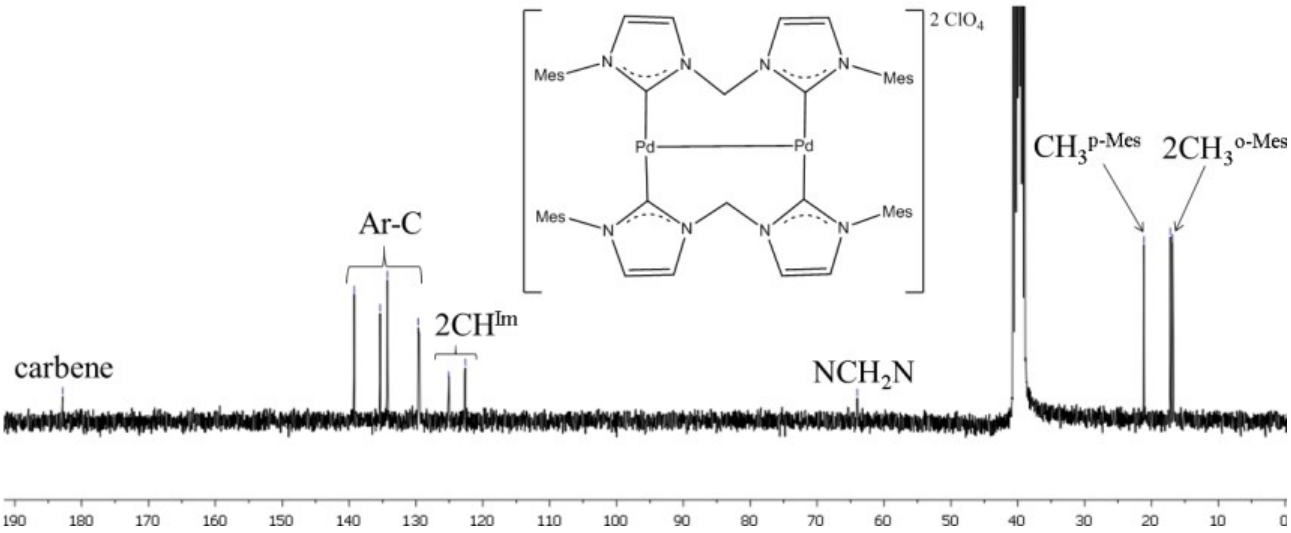

Figure S3: ^{13}C {^{1}H} NMR spectrum of Pd(I) dimer **3** in DMSO-d6 at 298 K

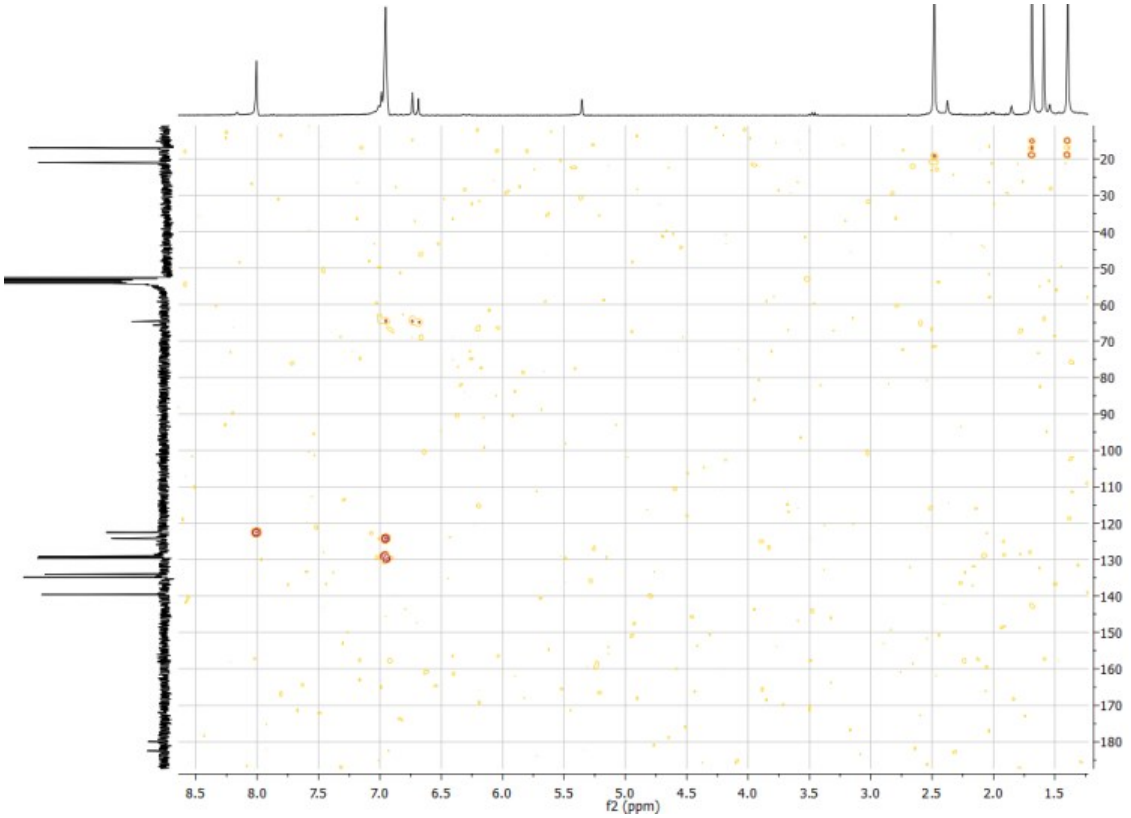

Figure S4: HSQC spectrum of Pd(I) dimer **3** in DMSO-d6 at 298 K

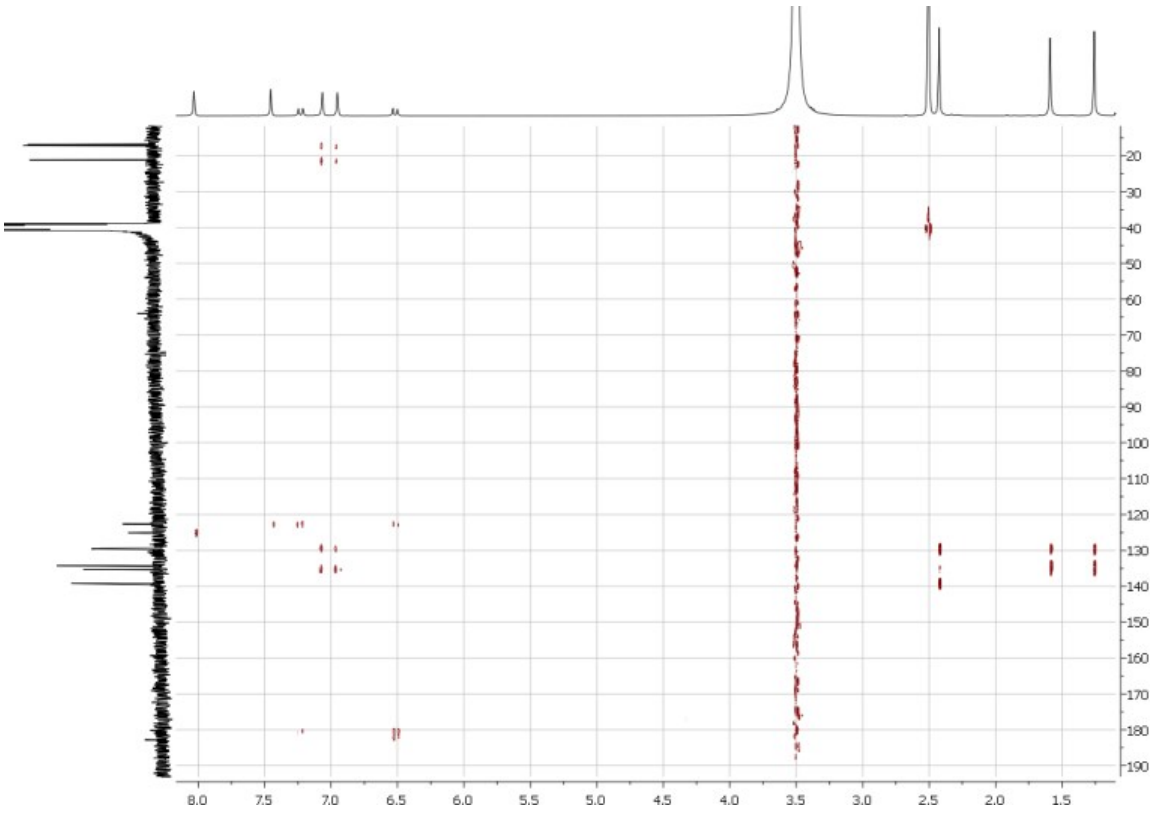

Figure S5: HMBC spectrum of Pd(I) dimer **3** in DMSO-d6 at 298 K

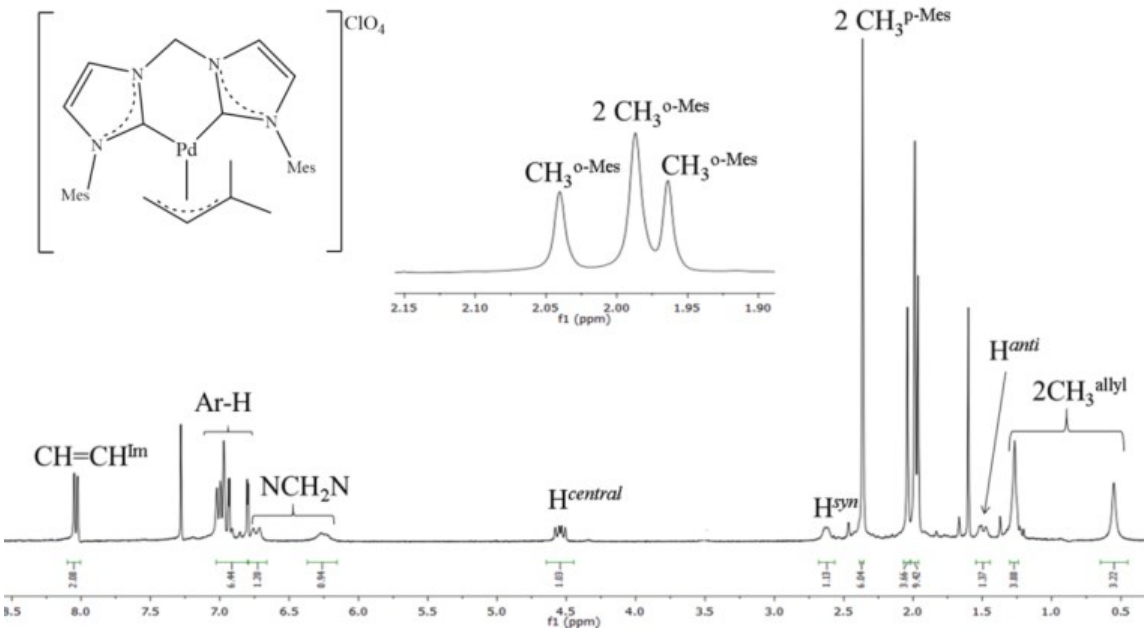

Figure S6: ^{1}H NMR spectrum of Pd(II)-(1,1-dimethyl-allyl) complex **2** in $CDCl_3$ at 298 K

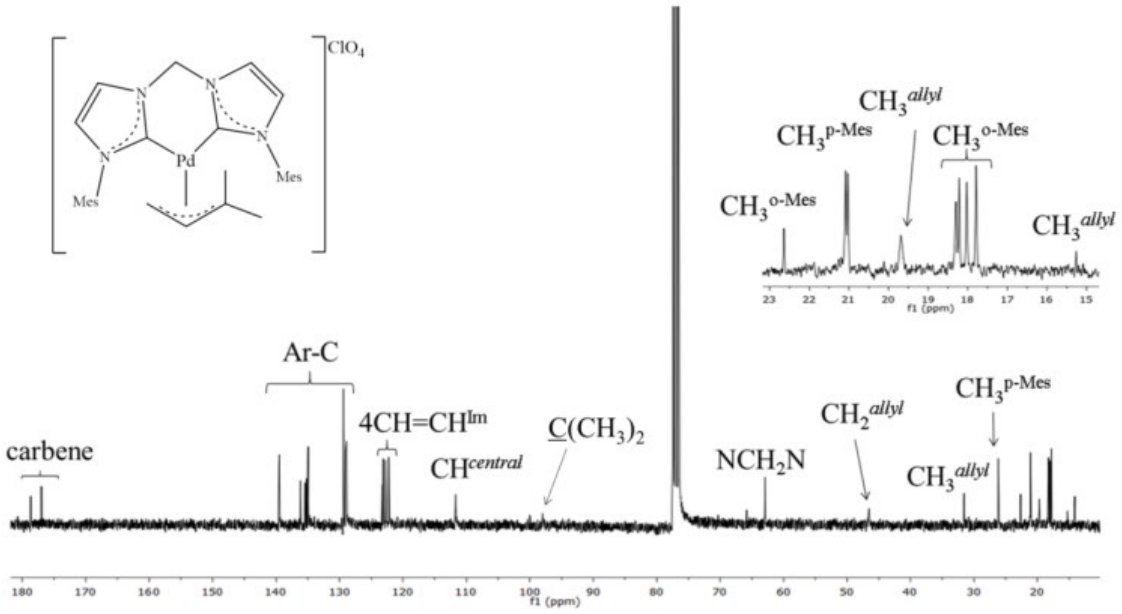

Figure S7: ^{13}C {^{1}H} NMR spectrum of Pd(II)-(1,1-dimethyl-allyl) complex **2** in $CDCl_3$ at 298 K

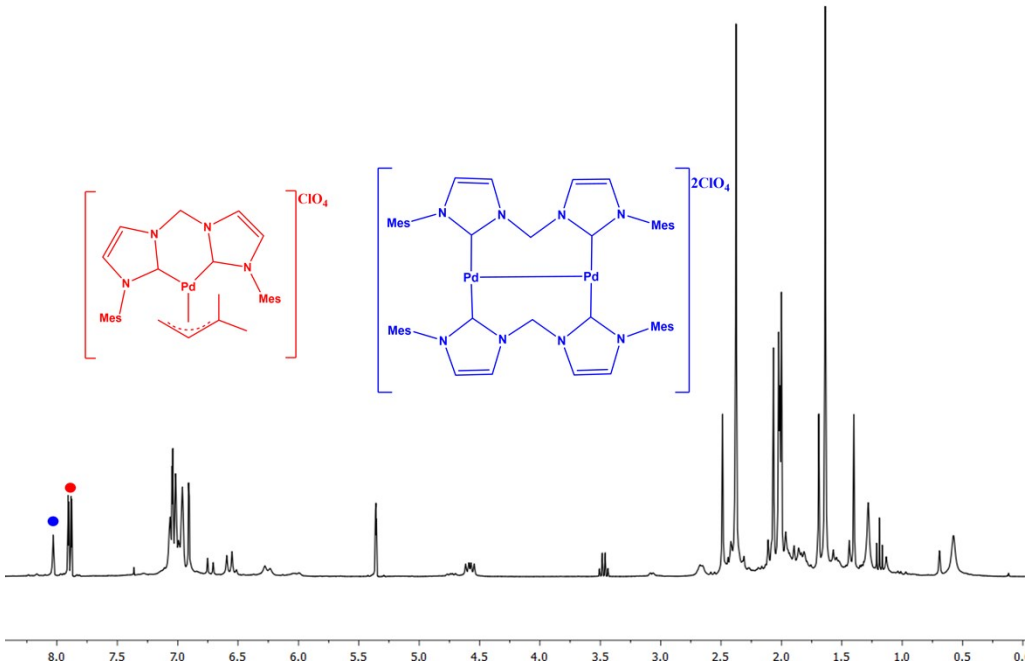

Figure S8: ^{1}H NMR spectrum in CD_2Cl_2 at RT for the reaction: 0.5 $[Pd(\mu\text{-}Cl)(1,1\text{-dimethylallyl})]_2$ + $[Ag_2(Mes\text{-}Im\text{-}CH_2\text{-}Im\text{-}Mes)Br_2]$ –> Pd(II)-(1,1-dimethyl-allyl) complex **2** + Pd(I) dimer **3** (Entry 1, Table S1)

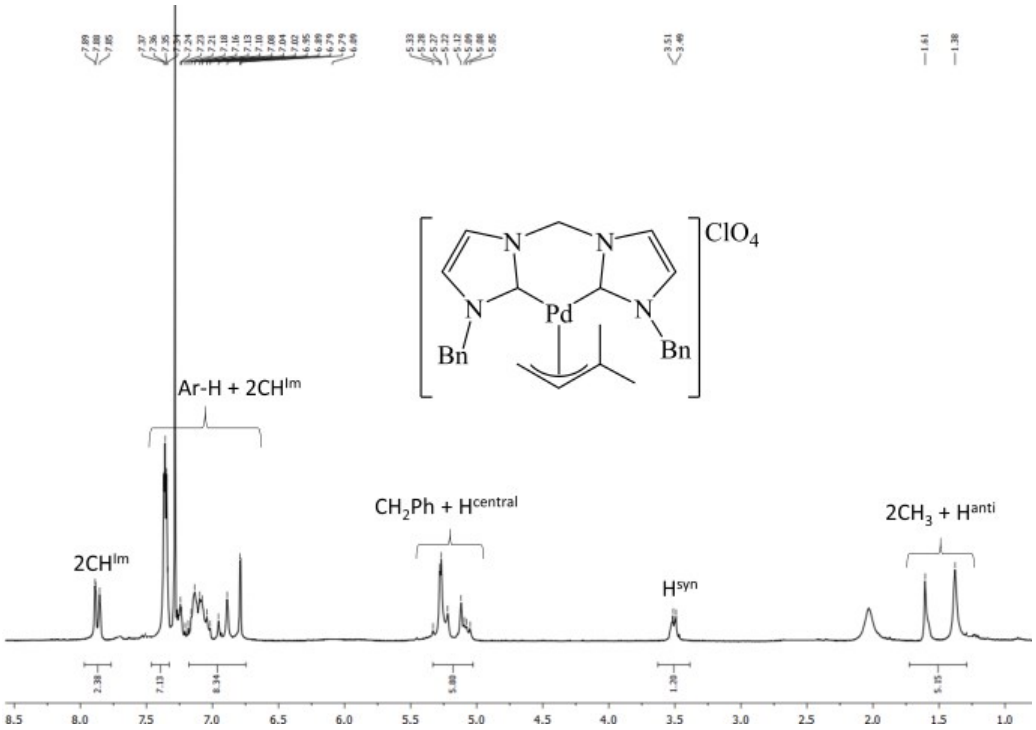

Figure S9: ^{1}H NMR spectrum in $CDCl_3$ at RT for the reaction: 0.5 [Pd(μ-Cl)(1,1-dimethylallyl)]$_2$ + [Ag_2(Bn-Im-CH_2-Im-Bn)Br_2] –> Pd(II)-(1,1-dimethyl-allyl) complex (Entry 2, Table S1)

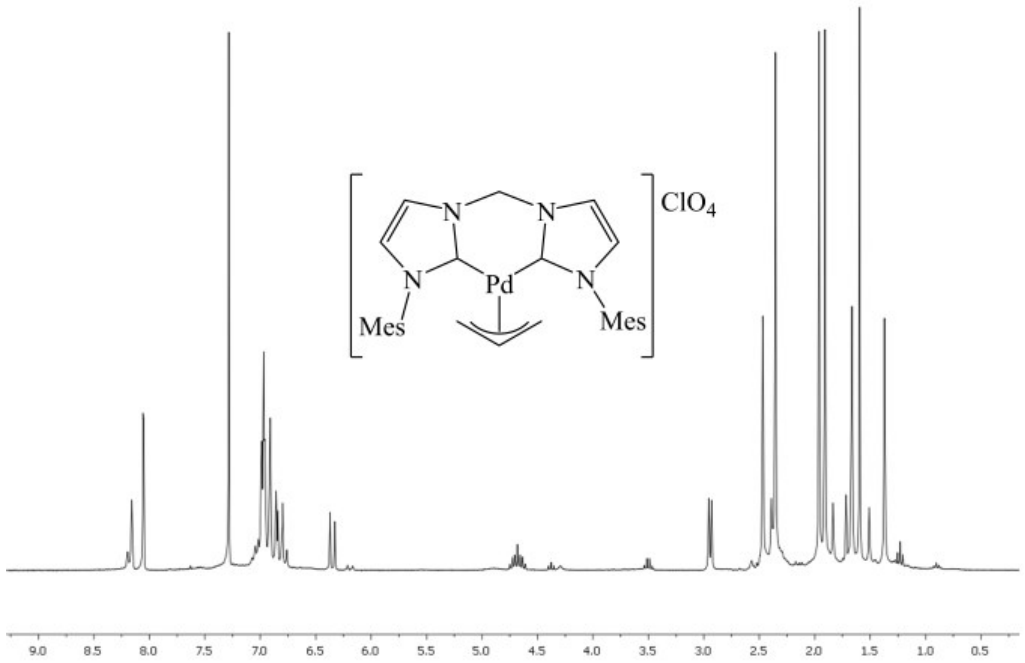

Figure S10: ^{1}H NMR spectrum in $CDCl_3$ at RT for the reaction: 0.5 [Pd(μ-Cl)(allyl)]$_2$ + [Ag_2(Mes-Im-CH_2-Im-Mes)Br_2] –> Pd(II)-(allyl) complex (Entry 3, Table S1)

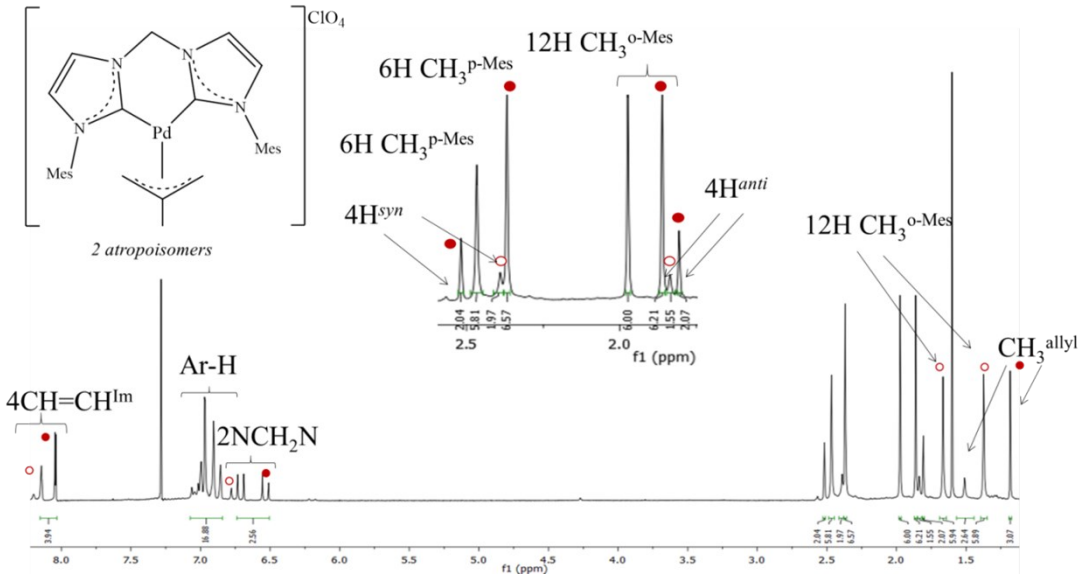

Figure S11: ^{1}H NMR spectrum in $CDCl_3$ at RT for the reaction: 0.5 $[Pd(\mu\text{-}Cl)(2\text{-methyl-allyl})]_2$ + $[Ag_2(Mes\text{-}Im\text{-}CH_2\text{-}Im\text{-}Mes)Br_2]$ –> Pd(II)-(2-methyl-allyl) complex (Entry 4, Table S1)

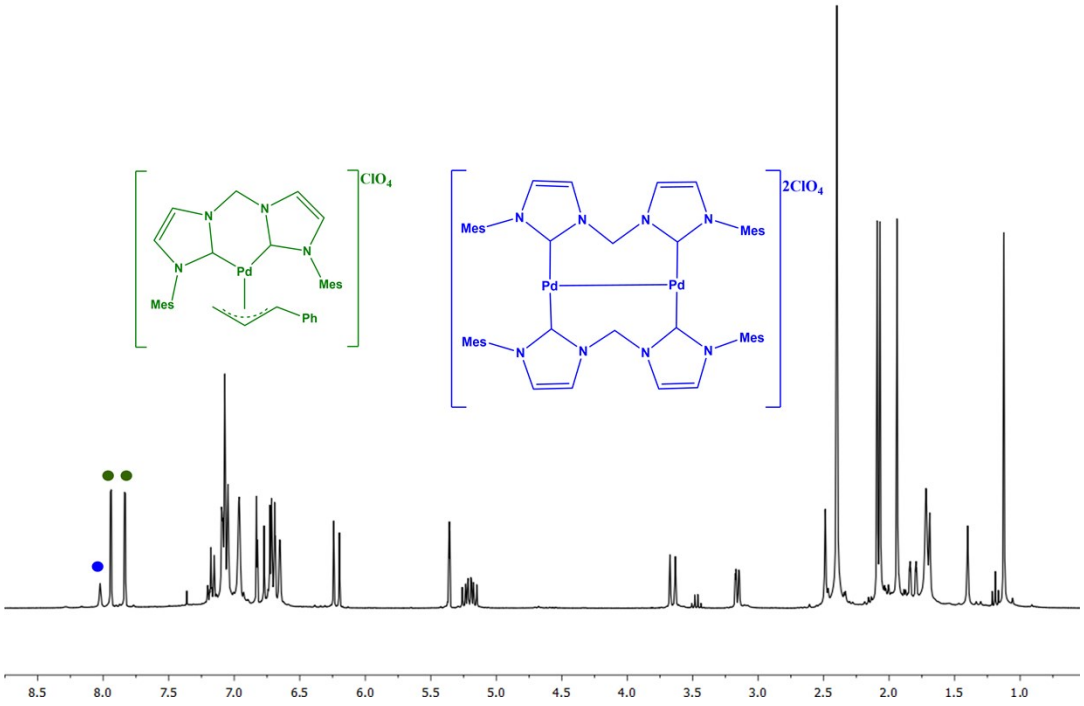

Figure S12: ^{1}H NMR spectrum in $CDCl_3$ at RT for the reaction: 0.5 $[Pd(\mu\text{-}Cl)(1\text{-phenyl-allyl})]_2$ + $[Ag_2(Mes\text{-}Im\text{-}CH_2\text{-}Im\text{-}Mes)Br_2]$ –> Pd(II)-(1-phenyl-allyl) complex + Pd(I) dimer **3** (Entry 5, Table S1)

Stability studies of complex 3

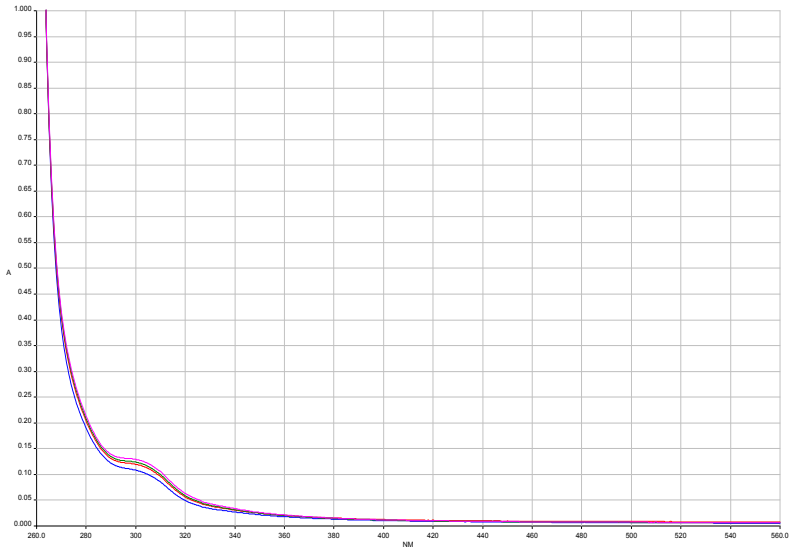

Figure S13: UV-Vis spectra of complex **3** in physiological solution at t = 0, 24h, 48h and 96h.

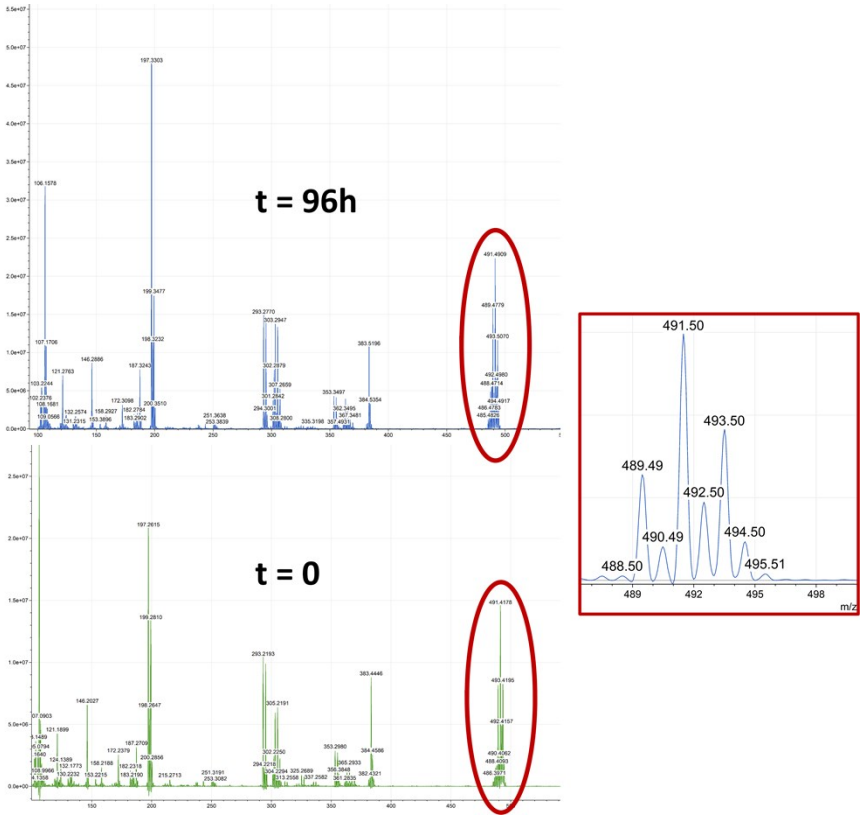

Figure S14: ESI-MS spectra of complex **3** in physiological solution at t = 0 and 96h.

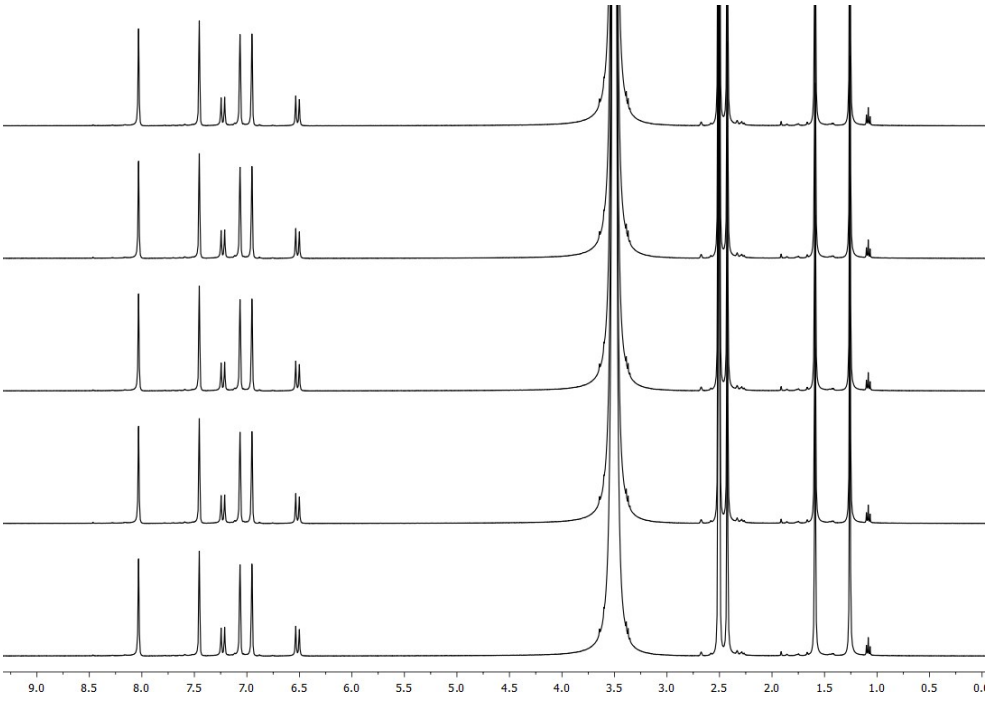

Figure S15: ^{1}H-NMR spectra (298K) of complex **3** in D_2O/DMSO (1:1) at t = 0, 24h, 48h, 72h and 96h.

Crystallographic data

Crystal Structure Determination

3 crystal data were collected at 100K at the XRD2 beamline of the Elettra Synchrotron, Trieste (Italy)[1], using a monochromatic wavelength of 0.620 Å. The data sets were integrated and corrected for Lorentz, absorption and polarization effects using XDS package.[6] The structures were solved by direct methods using SHELXT program[7] and refined using full−matrix least−squares implemented in SHELXL−2018/3.[8]

Thermal motions for non−hydrogen atoms, with occupancies greater than 50%, have been treated anisotropically and hydrogens have been included on calculated positions, riding on their carrier atoms. Geometric restrains (DFIX and DANG) have been applied to disordered chloroform molecules and ClO_4^- counterions. The Coot program was used for structure building.[9] The crystal data are given in Table S1. Pictures were prepared using Ortep3[10] and Pymol[11] softwares.

Crystallographic data has been deposited at the Cambridge Crystallographic Data Centre and allocated the deposition number CCDC 2006223. These data can be obtained free of charge via https://www.ccdc.cam.ac.uk/structures.

Table S2: Crystallographic data.

Compound	**3**
Formula	$[Pd_2(C_{25}H_{28}N_4)_2](ClO_4)_2 \cdot 3CHCl_3$
M/g·mol^{-1}	1538.83
Space group	$P2_1/n$
Crystal system	Monoclinic
a/Å	12.180(2)
b/Å	15.906(3)
c/Å	33.211(7)
α/°	90
β/°	93.15(3)
γ/°	90
V/Å^3	6424(2)
Z	4
T/K	100
D_c/g·cm^{-3}	1.591
F(000)	3104
μ(0.7Å)/cm^{-1}	7.29
Measured Reflections	126639
Unique Reflections	26198
R_{int}	0.0477
Obs. Refl.ns [I≥2σ(I)]	20213
θ_{min}- θ_{max}/°	1.24 – 30.01
hkl ranges	-19,19; -25,25; -53,53
R(F^2) (Obs.Refl.ns)	0.0529
wR(F^2) (All Refl.ns)	0.1534
No. Variables	806
Goodness of fit	1.034
$\Delta\rho_{max}$; $\Delta\rho_{min}$ /e·Å^{-3}	1.38; -1.70
CCDC Deposition N.	2006223

Table S3: Selected bond distances and angles (Å and °) for **3** palladium coordination spheres (naming scheme is reported in Fig.S13). Equivalent CCDC 778437-77844[12] average values are reported for comparison.

3					**Average CCDC 778437-778441[12]**			
Distances	**(Å)**	**Angles**	**(°)**		**Distances**	**(Å)**	**Angles**	**(°)**
Pd_1-C2_3	2.084(2)	C2_3-Pd_1-C12_4	170.40(9)		Pd_1-C2_3	2.05(1)	C2_3-Pd_1-C12_4	167.3(5)
Pd_1-C12_4	2.077(2)	C2_3-Pd_1-Pd_2	103.05(7)		Pd_1-C12_4	2.01(1)	C2_3-Pd_1-Pd_2	105.3(4)
Pd_2-C2_4	2.088(2)	C12_4-Pd_1-Pd_2	86.18(7)		Pd_2-C2_4	2.05(1)	C12_4-Pd_1-Pd_2	86.8(4)
Pd_2-C12_3	2.092(2)	C2_4-Pd_2-C12_3	171.64(9)		Pd_2-C12_3	2.01(1)	C2_4-Pd_2-C12_3	167.4(5)
Pd_1-Pd_2	3.163(1)	C2_4-Pd_2-Pd_1	101.74(7)		Pd_1-Pd_2	2.77(1)	C2_4-Pd_2-Pd_1	104.6(4)
		C12_3-Pd_2-Pd_1	86.45(7)				C12_3-Pd_2-Pd_1	86.7(4)

Table S4: Pd-Pd and Pd-C(carbene) distances (Å) for **3** and some Pd(I) dimers previously reported in literature.

Complex **3**		**CCDC 778437-778441**[12]		**CCDC 1030341**[13]		**CCDC 964688**[14]		**CCDC 1424770**[15]	
Distances	**(Å)**	**Distances**	**(Å)**	**Distances**	**(Å)**	**Distances**	**(Å)**	**Distances**	**(Å)**
Pd_1-C2_3	2.084(2)	Pd_1-C2_3	2.05(1)	Pd(1)-C(13)	2.031(3)	Pd1-C9	2.0539(17)	Pd1−C1	1.98(3)
Pd_1-C12_4	2.077(2)	Pd_1-C12_4	2.01(1)	Pd(2)-C(10)	2.039(3)	Pd1-C7	2.067(15)	Pd1'−C1'	1.98(3)
Pd_2-C2_4	2.088(2)	Pd_2-C2_4	2.05(1)						
Pd_2-C12_3	2.092(2)	Pd_2-C12_3	2.01(1)						
Pd_1-Pd_2	3.163(1)	Pd_1-Pd_2	2.77(1)	Pd(1)-Pd(2)	2.6062(4)	Pd1-Pd1	2.7050(3)	Pd1-Pd1'	2.6574(5)

X-ray diffraction analysis – Additional comments

Crystalline form of **3** contains one crystallographically independent palladium complex showing a dinuclear cluster in a planar coordination environment with a pseudo-C_2 symmetry (Figure S13, Table S2). The crystallographic asymmetric unit (A.S.U. - Figure S14) bears 2 perchlorate counterions which implies an overall "+2" **3** charge (shortest ions distance: $d_{Pd\cdots O}$ = 3.651(6) Å). The two palladium centers show substantially equivalent geometrical parameters, with minor differences related to different intramolecular contacts of neighbour mesitylene substituents (ring centroids distances of neighbour aromatic substituents are 4.162(2) Å for "Pd_2" and 5.022(2) Å for "Pd_1") and different intermolecular packing interactions. The molecular structure of **3** closely resembles its monocationic counterpart, previously published[12] with slightly longer metal bonds (Figure S15, Table S2). The overlaps among $[Pd_2(NHC)_2]^{n+}$ models show an average R.M.S.D. of ~0.7 Å, with largest shifts on lateral mesitylene substituents.

Crystal packing of **3** shows hydrophobic contacts involving CH···π and weak intermolecular π···π interactions, among neighbour aromatic NHC sidechains. Three chloroform molecules, coordinated to perchlorate ions through weak C-H···O-Cl hydrogen bonds (shortest one is $d_{C\cdots O}$ = 2.949(7) Å), have been located in the A.S.U. filling empty voids.

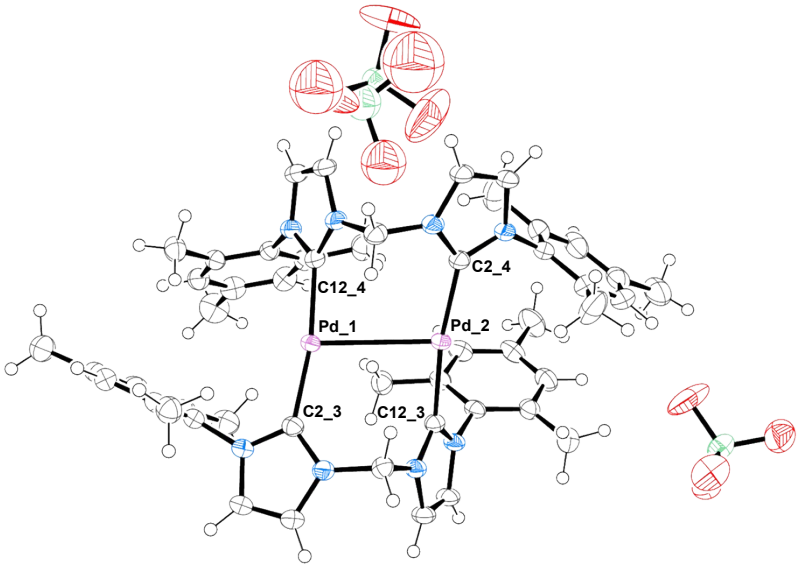

Figure S16: Ellipsoid representation of **3** (50% probability). Atom labels in use for Pd coordination spheres, are reported.

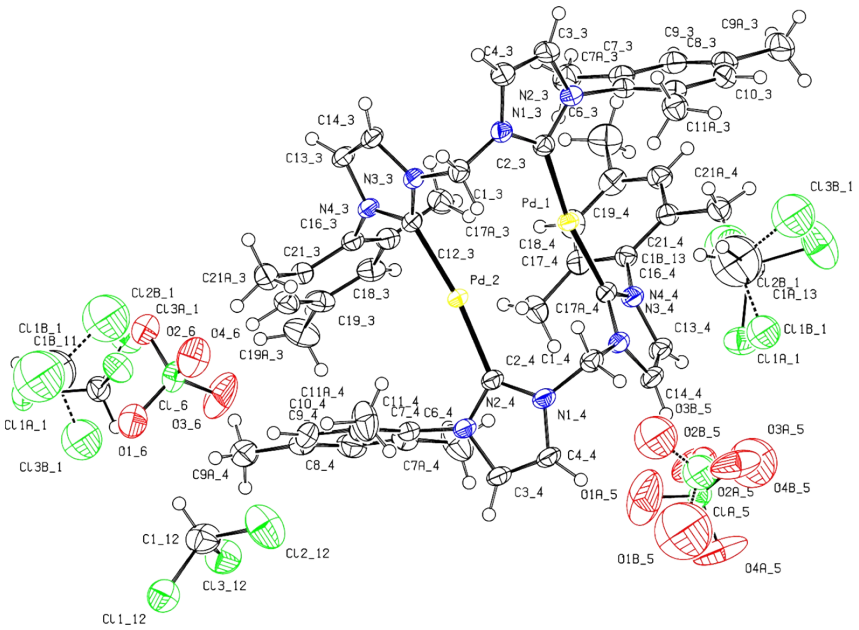

Figure S17. Ortep representation of **3** crystallographic asymmetric unit (ellipsoids radii corresponding to 50% probability). Atom labels in use are reported.

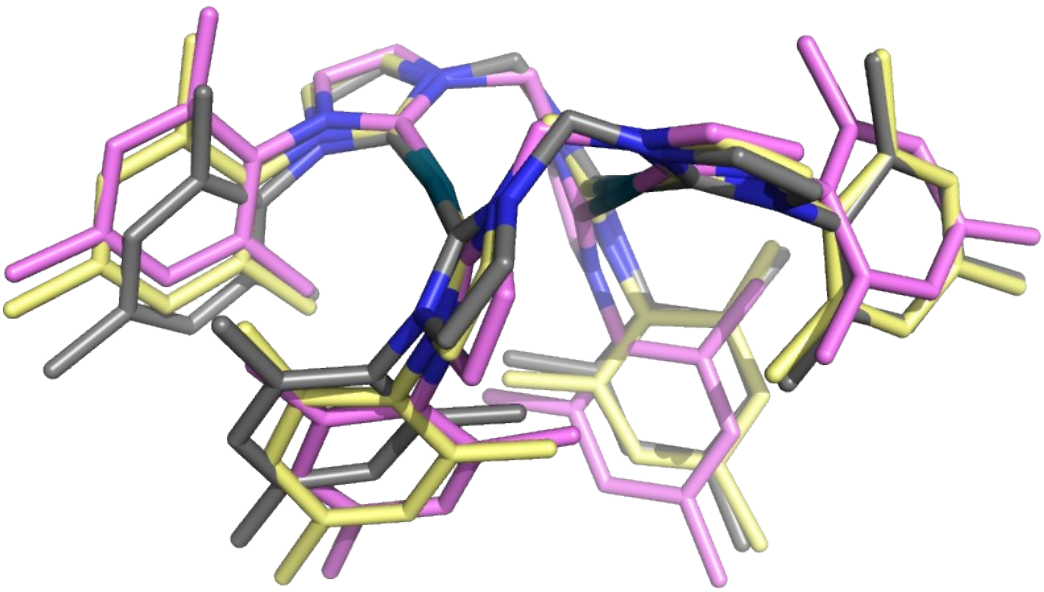

Figure S18. Stick representation of **3** (grey sticks) overlapped to CCDC 778441 (yellow sticks) and CCDC 778440 (purple sticks)[12], showing the equivalent conformations adopted by NHC ligands (R.M.S.D. are 0.52 Å and 0.93 Å respectively). Hydrogen atoms omitted for clarity.

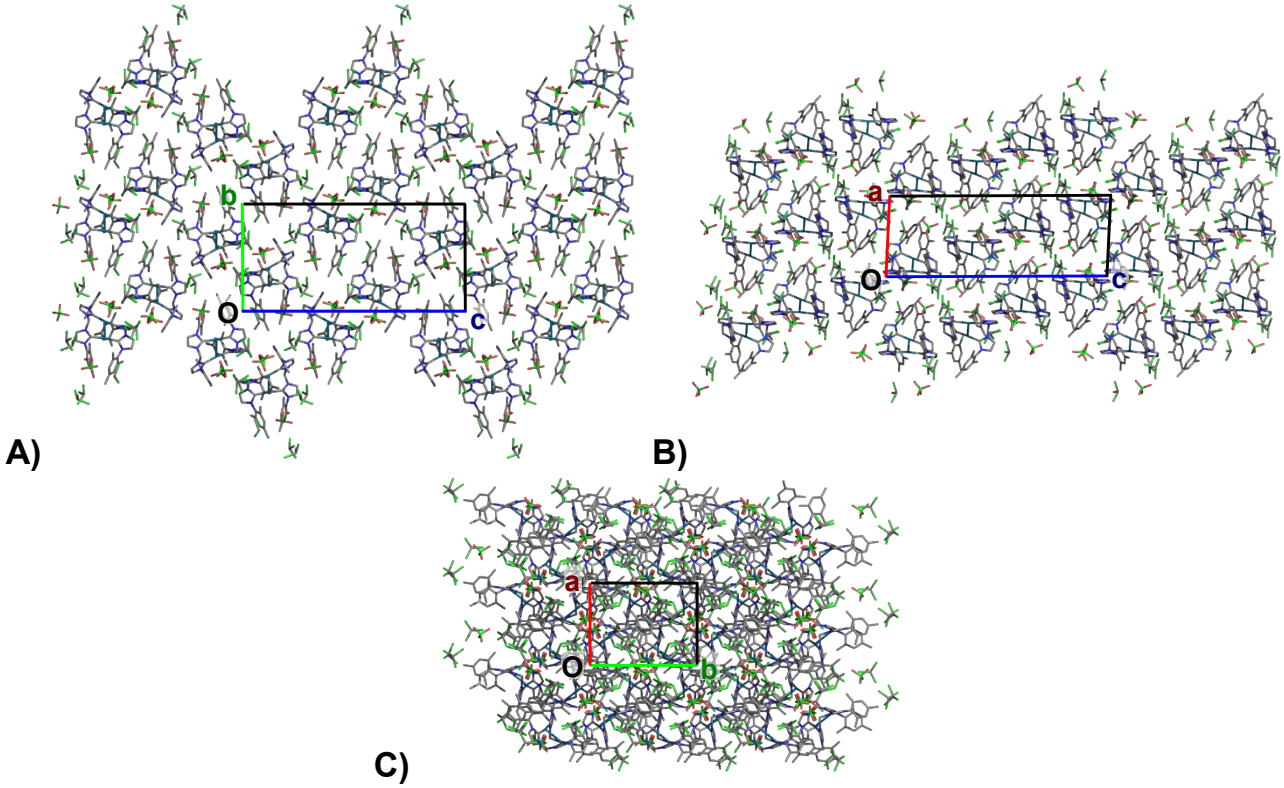

Figure S19. **3** crystal packing views along crystallographic *a*, *b* and *c* axis. Hydrogens omitted for clarity.

Computational studies

All DFT calculations were performed using the Gaussian09 package.[16] The geometry optimizations were performed using the PBE0 functional[17] including Becke-Johson damped D3 dispersion.[18] The electronic configuration of all non-metal elements was described with the Ahlrichs split-valance polarization basis function SVP[19] while the SDD[20] pseudopotential and its associated double-ζ basis set was employed for the Pd atom. Single point energy calculations were carried out using TZVP[19] and SDD basis sets for non-metal atoms and the Pd, respectively. Optimizations were performed in gas phase, and solvation effects were incorporated through single-point energy calculations using the SMD[21] continuum solvation model with the solvent parameters for dichloromethane (ε = 8.93). The singlet open-shell state having a biradical character was handled with a broken symmetry approach, and it is labelled as ^{1}BS.

Table S5. Relative electronic energies for **3** along with spin density populations at fixed Pd-Pd bond distance.

Electronic State	ΔE	ρ_{Pd1} [a]	ρ_{Pd2} [a]	d(Pd-Pd) [b]
^{1}BS(1,1) [c]	0.0	0.58	-0.58	3.16
Closed-shell singlet	4.1	0.00	0.00	3.16
Triplet	6.6	0.78	0.77	3.16

[a] : Spin density population localized over Pd atoms.
[b] : Bond distance between two Pd centers in Å.
[c] : Broken symmetry solution for the antiferromagnetically coupled Pd atoms, overall with an open-shell singlet.

Table S6. Relative electronic energies for **3** along with spin density populations at relaxed Pd-Pd bond distance.

Electronic State	ΔE	ρ_{Pd1} [a]	ρ_{Pd2} [a]	d(Pd-Pd) [b]
^{1}BS(1,1) [c]	0.0	0.00	0.00	2.55
Closed-shell singlet	0.0	0.00	0.00	2.55
Triplet	15.4	0.76	0.76	2.83

[a] : Spin density population localized over Pd atoms.
[b] : Bond distance between two Pd centers in Å.
[c] : Broken symmetry solution for the antiferromagnetically coupled Pd atoms, overall with an open-shell singlet.

The energy difference between the constrained and relaxed geometries is 8.0 kcal/mol for the singlet state due to the considerable contraction of the Pd-Pd bond from 3.16 to unrealistic value of 2.55 Å. Though the triplet state is ruled out based on the experimental NMR analysis and DFT calculations, the negligible energy difference between the associated constrained and fully relaxed structures (0.8 kcal/mol) can be explained by relatively insignificant change in Pd-Pd bond from 3.16 to 2.83 Å. Moreover, inclusion of two counterions gives rise to a 1.0 kcal/mol energy difference between two structures with a fixed and relaxed Pd-Pd distance where the latter reduces to 2.70 Å. Taken all together, Pd(I)-Pd(I) dimer is best described as a BS singlet for the experimentally reported crystal structure.

Analysis of the HOMO and LUMO shown in Figure S20, indicates a strong overlap between the two metal centers further supported by the strong antiferromagnetic coupling as presented in panel b and implies high covalency between two Pd(I) atoms.

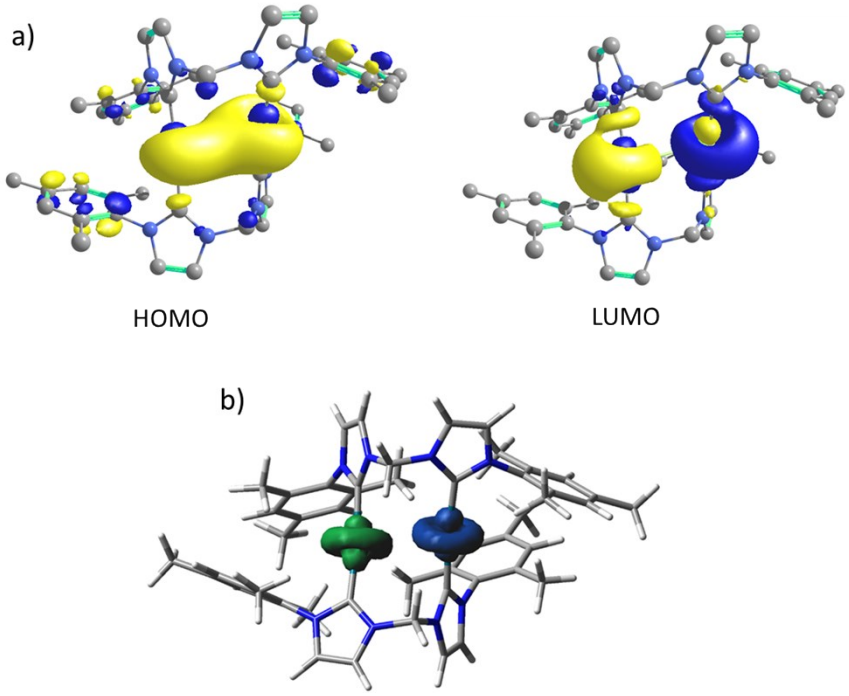

Figure S20. HOMO, LUMO and spin density map for the ^{1}BS(1,1) solution.

Biological studies

Cell viability assays

Cells were grown in accordance with the supplier and maintained at 37°C in a humidified atmosphere of 5% carbon dioxide. Five hundred cells were plated in 96 wells and treated with six different concentration (0.001, 0.01, 0.1, 1, 10 and 100 µM) of palladium compounds. After 96 hours from the treatment cell viability was measured with CellTiter-Glo® Luminescence assay (Promega, WI, US) with a Tecan M1000 instrument. IC_{50} values were calculated from logistical dose response curves. Averages were obtained from triplicates, and error bars are standard deviations.[22]

Organoids isolation and culture

Mouse liver organoids were isolated from 8-week-old C57/BL6 mice following the protocol described by Stappenbeck.[23] Summarizing, a piece of liver was dissected and incubated with collagenase 2 mg/mL for 30'. After the enzymatic digestion, the tissue was transferred into a clean 15 mL tube with 10 mL of washing medium and centrifugated at 0.5xg. Supernatant was discarded, the pellet was resuspended in 10 µL of Cultrex® BME (Trevigen, MD, US) and plated in a 24 mw. After solidification of the matrix, 500 µL of medium was added to each well.

Patient derived organoids (PDO) were obtained from totally anonymized surgical specimens. However, biobank informed consent for research purposes was available to collect the samples. Tissues were processed and cultured using the protocol described for the isolation of mouse organoids. Mouse liver was collected post mortem to generate organoids following the Institutional guideline at Centro di Riferimento Oncologico of Aviano (approved by Italian Ministry of Health; number: 148/2016-PR).

Toxicity tests on mouse liver organoids

Toxicity test on mouse liver organoids was performed treating organoids (five replicates) on 96-MW with the Pd(I) dimer **3** ranging from 100 µM to 0.01 µM for 96 hours. As positive control, we used cisplatin starting from 330 µM to 0.03 µM. The cytotoxicity was correlated with the cell viability evaluated by CellTiter-Glo® Luminescence assay (Promega, WI, US) with an Infinite 200 PRO instrument (Tecan, Switzerland).

PDO drug efficacy test

PDO drug efficacy tests were performed at passage zero. PDO were plated on 96-MW and treated with **3** ranging from 100 µM to 1 nM, carboplatin ranging from 200 µM to 2 nM and paclitaxel from 20 µM to 0.2 nM for 96 hours. Cell viability was evaluated by CellTiter-Glo®Luminescence assay (Promega, WI, US) with an Infinite200 PRO instrument (Tecan, Switzerland). IC_{50} values were calculated with Prism® (Version 8.0, GraphPad software Inc.) IC_{50} values were calculated from logistical dose response curves. Averages were obtained from quintuplicates, and error bars are standard deviations.

DNA damage and Cytochrome C release assays

A2780 and HeLa cells were seeded at a density of $2 \cdot 10^5$ cells/mL on coverslip glass (pretreated with poly-D-Lysine, 1 mg/mL) inserted in 6-well plates. After overnight culture at 37 °C and 5% CO_2, cells were treated with different concentrations of Pd(I) dimer **3** (10, 25, 75 nM for A2780 and 2, 3.5 and 10 µM for HeLa) or cisplatin (10 µM) for 3, 6, and 12 h. Cells were fixed in 4% paraformaldehyde/PBS (20 min, RT), permeabilized with 0.3% Triton X-100/PBS (15 min, RT) and blocked in 8% BSA/PBS (1 h, RT). Cells were stained with mouse monoclonal anti-phosphohistone pS139H2A.X antibody (1:100 dilution in 1% BSA/PBS, at 4°C, overnight) or with mouse monoclonal anti-cytochrome C (6H2.B4) antibody (1:100 dilution in 1% BSA/PBS, at 4 °C, overnight) which were obtained respectively from Millipore (Cat. # 05e636; Burlington, MA, USA) and Cell Signaling Technology (Cat. # 12963; Danvers, MA, USA), and labeled with secondary antibody (Alexa Fluor® 488 dye, 1:1000 dilution, RT, 2 h) obtained from Cell Signaling Technology (Cat. # 4408; Danvers, MA, US).

To visualize DNA, cells were stained with DAPI 1 mg/mL (1:10000 dilution in PBS, RT, 1 min). Cells were washed three times with PBS after all incubations. All the coverslips were mounted in fluorSave™ reagent (Cat. # 345789; Millipore: Burlington, MA, USA)-

The cells were examined with a Leica DM5500B fluorescence microscope with a X-Cite 120 PC Q lamp and the images were analyzed with Cytovision software.

Mitochondrial membrane potential assay

A2780 cell line were seeded at a density of $2 \cdot 10^5$ cells/mL and inserted in 6-well plates. After incubation overnight at 37 °C in 5% CO_2, cells were treated with different concentrations of Pd(I) dimer **3** (10, 25, 75 nM), cisplatin (10 μM) or H_2O_2 (1 mM) for (30 min, 1h, 2h and 3 h).

Working staining solution was prepared from the JC-1 powdered dye provided from Invitrogen (Cat. # T3168; Waltham, MA, US) in dimethyl sulfoxide (DMSO) at 1 mg/mL, which was then added to the cells (10 μg/mL, previously diluted in culture medium, according to JC-1 cell staining conditions). Incubation was carried out at 37°C in 5 % CO_2 incubator for 10 minutes. Cells were washed with 2× DPBS, examined with a Nikon Eclipse Ti-U fluorescence microscope, and the images were analysed with NIS Elements software version 3.0 (Nikon: Shinagawa, Tokyo, Japan).

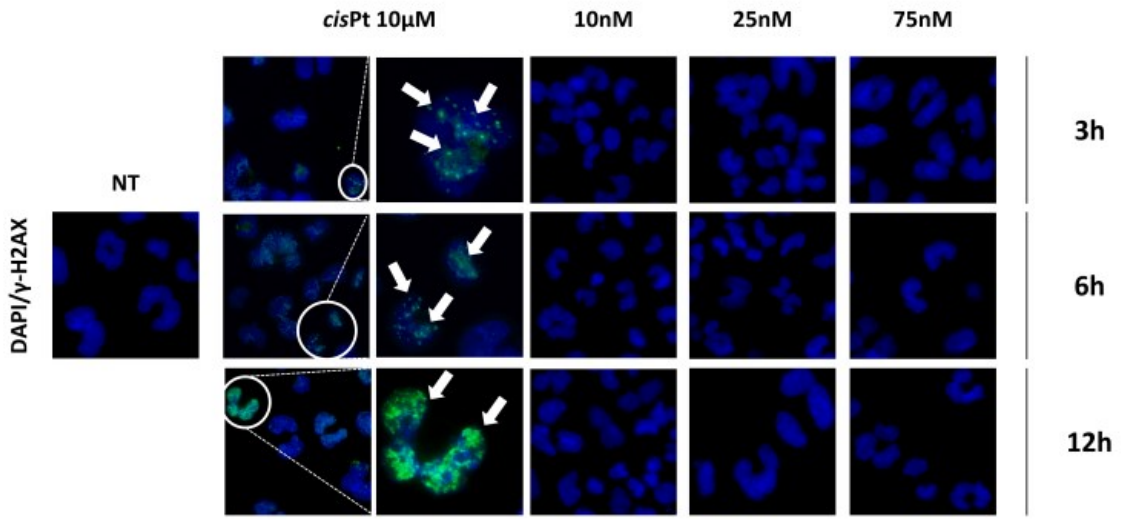

Figure S21: Assay on DNA damage after incubation of A2780 cell line with Pd(I) dimer **3** (10, 25 and 75 nM) and CisPt (10 µM). Arrows indicate nuclear foci of Ser139-Histone H2AX. Pictures taken at 63× magnification.

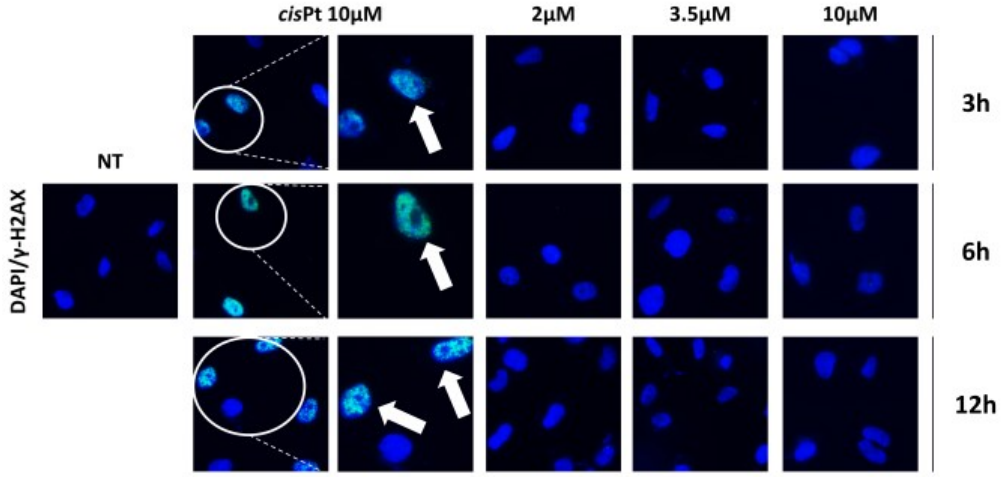

Figure S22: Assay on DNA damage after incubation of HeLa cell line with Pd(I) dimer **3** (2, 3.5 and 10 µM) and CisPt (10 µM). Arrows indicate nuclear foci of Ser139-Histone H2AX. Pictures taken at 63× magnification.

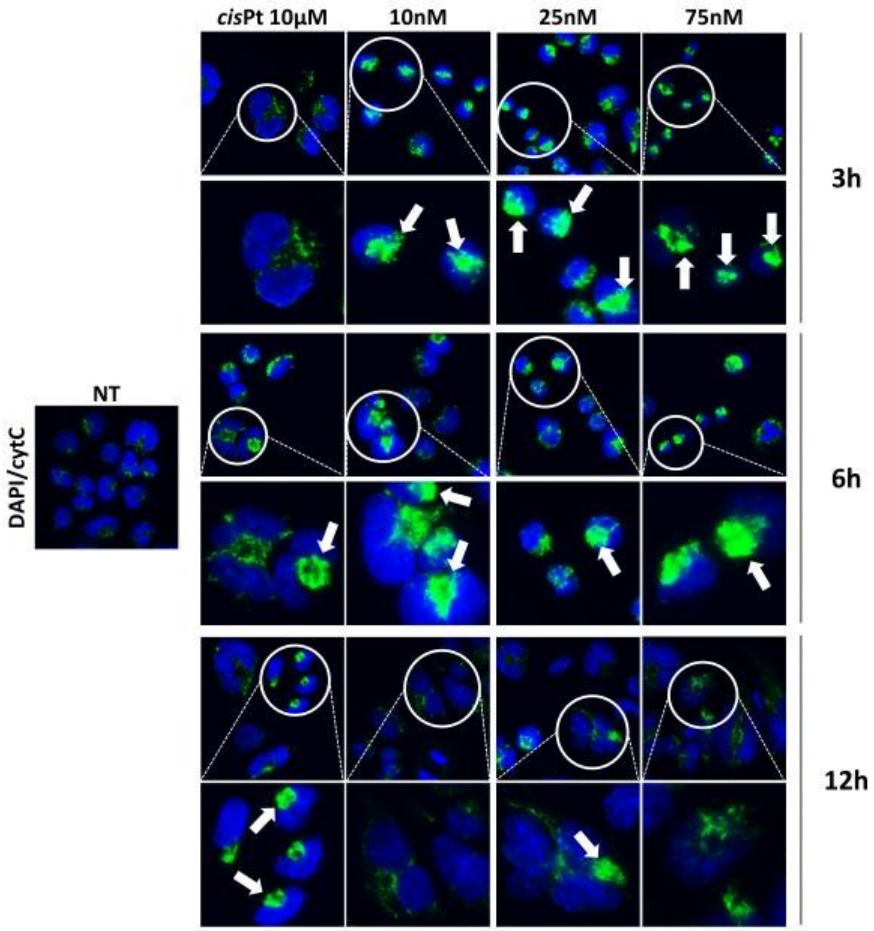

Figure S23. Immunofluorescence analysis of cytochrome C release after incubation of A2780 cells with Pd(I) dimer **3** (10, 25 and 75 nM) and CisPt (10 µM). Arrows indicate cytochrome C release. Pictures taken at 63× magnification.

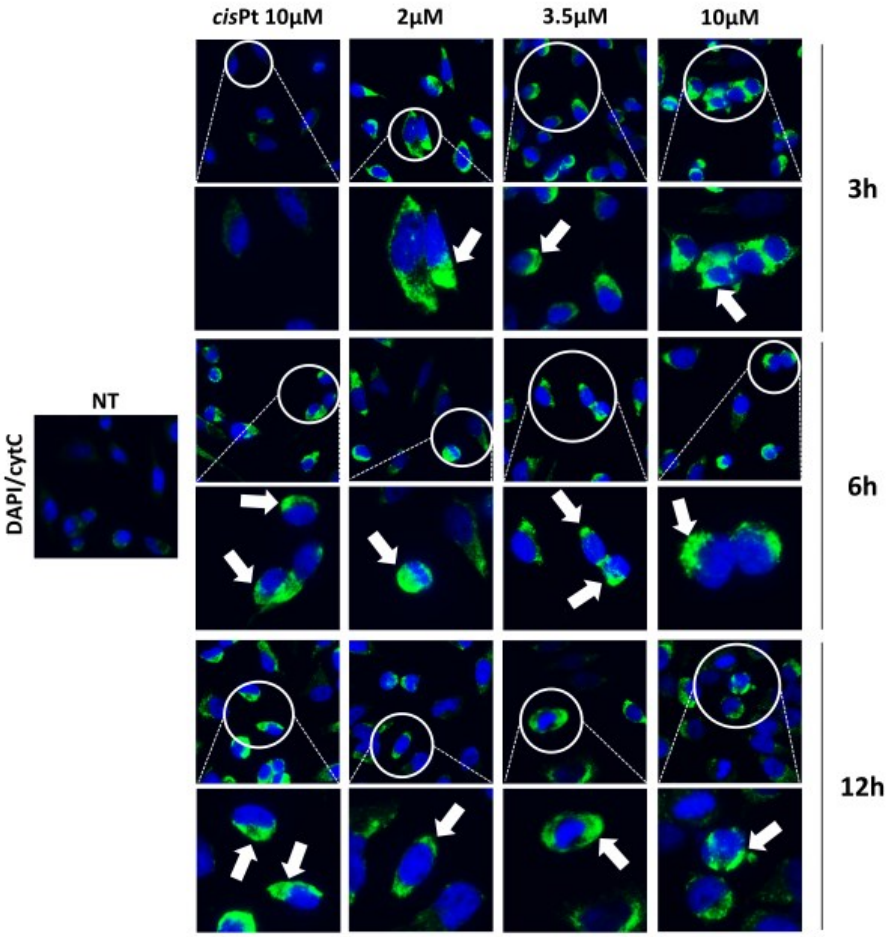

Figure S24: Immunofluorescence analysis of cytochrome C release after incubation of HeLa cells with Pd(I) dimer **3** (2, 3.5 and 10 µM) and CisPt (10 µM). Arrows indicate cytochrome C release. Pictures taken at 63× magnification.

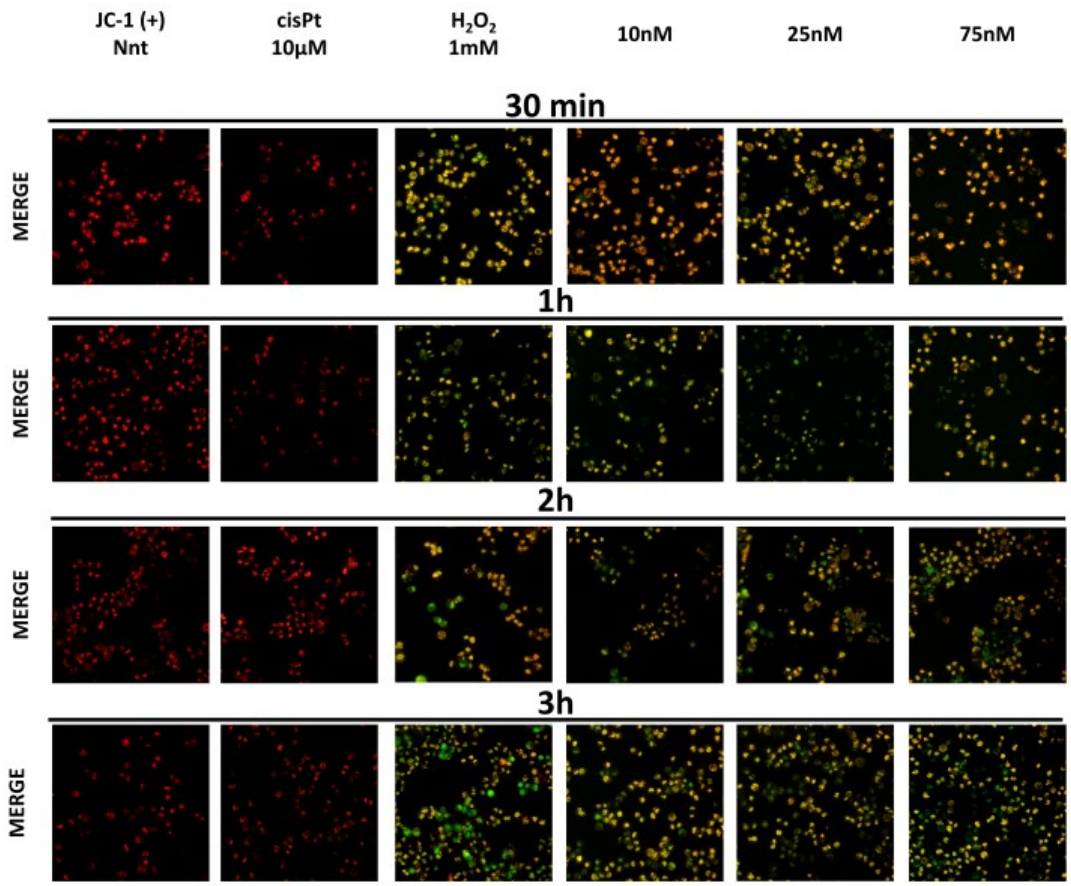

Figure S25: Effect of **3** (10, 25 and 75 nM), Cisplatin (10 µM) and H_2O_2 (1 mM) on mitochondrial potential of A2780 cell line after incubation for 30 min, 1, 2 and 3 hours with JC-1 dye. Pictures taken at 30× magnification.

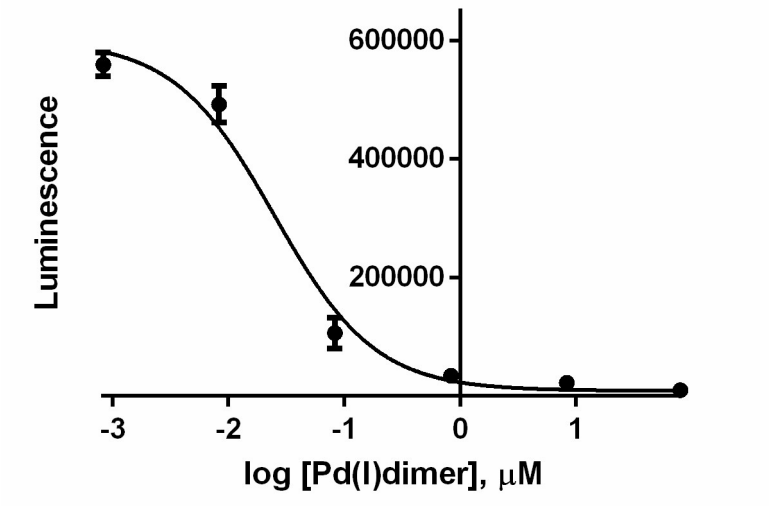

Figure S26: IC_{50} graph of A2780 cell line treated with Pd(I) dimer **3**.

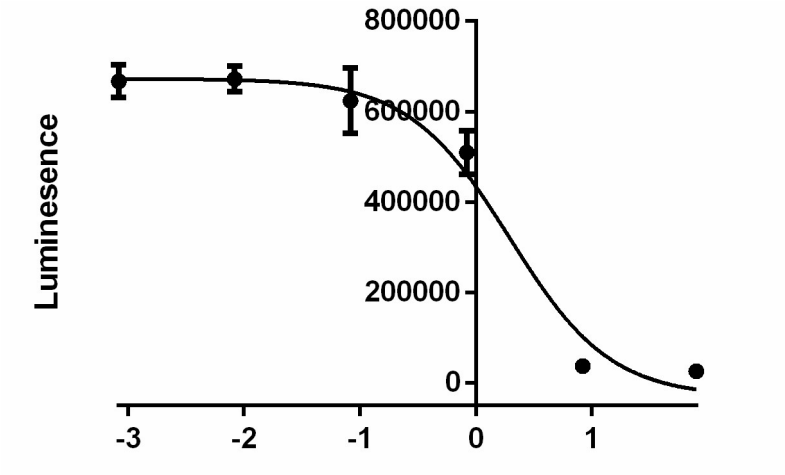

Figure S27: IC_{50} graph of A2780*cis* cell line treated with Pd(I) dimer **3**.

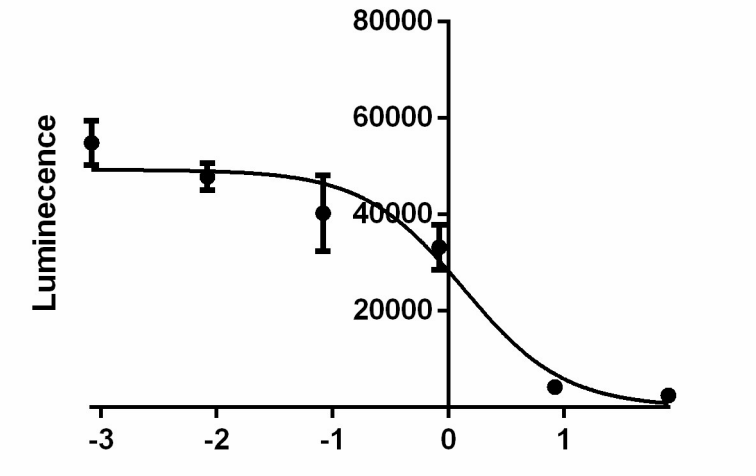

Figure S28: IC_{50} graph of OVCAR5 cell line treated with Pd(I) dimer **3**.

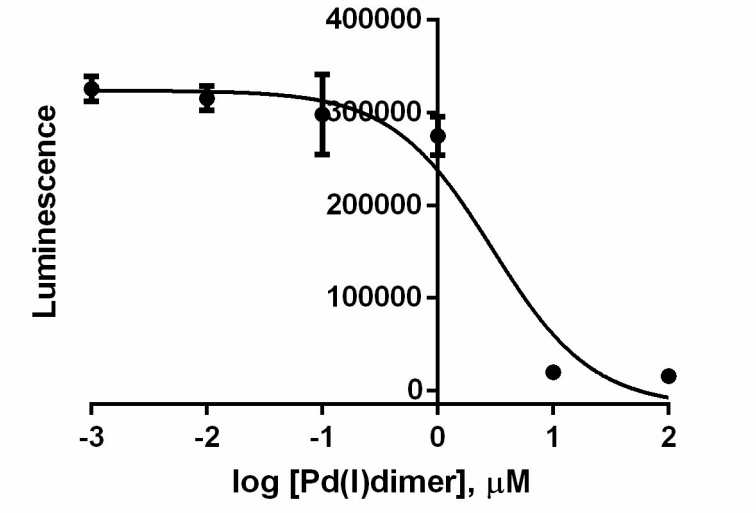

Figure S29: IC_{50} graph of OVCAR3 cell line treated with Pd(I) dimer **3**.

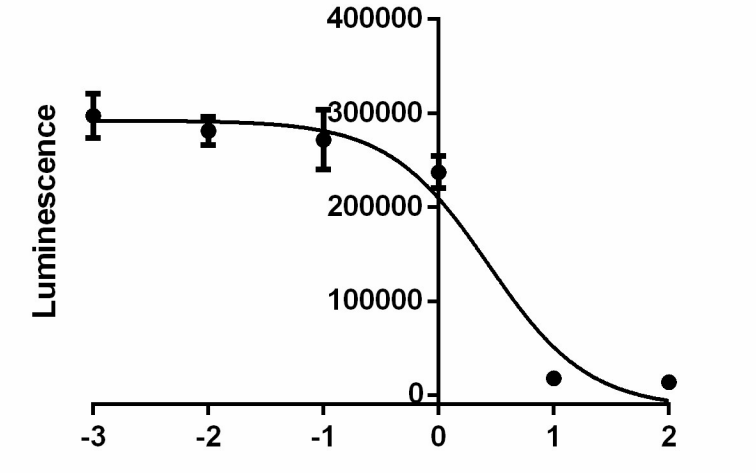

Figure S30: IC_{50} graph of KURAMOCHI cell line treated with Pd(I) dimer **3**.

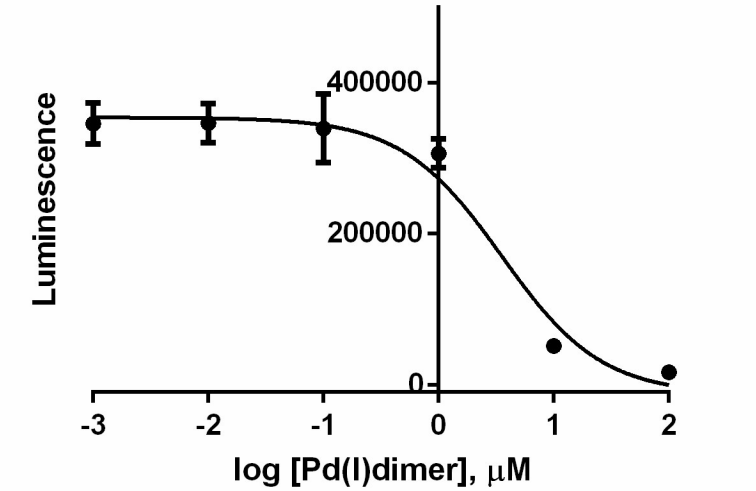

Figure S31: IC_{50} graph of HeLa cell line treated with Pd(I) dimer **3**.

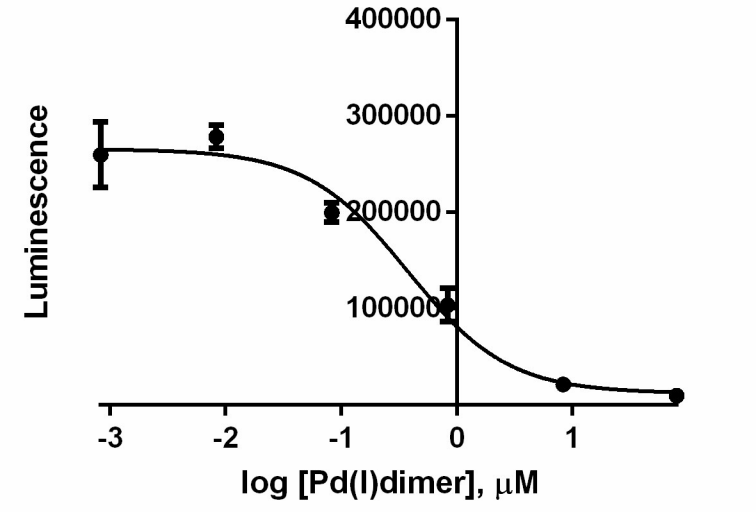

Figure S32: IC_{50} graphs of A549 cell line treated with Pd(I) dimer **3**.

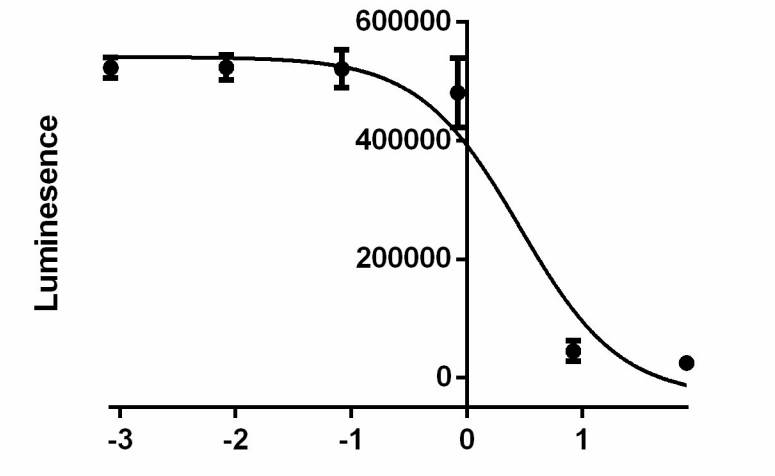

Figure S33: IC_{50} graph of DLD1 cell line treated with Pd(I) dimer **3**.

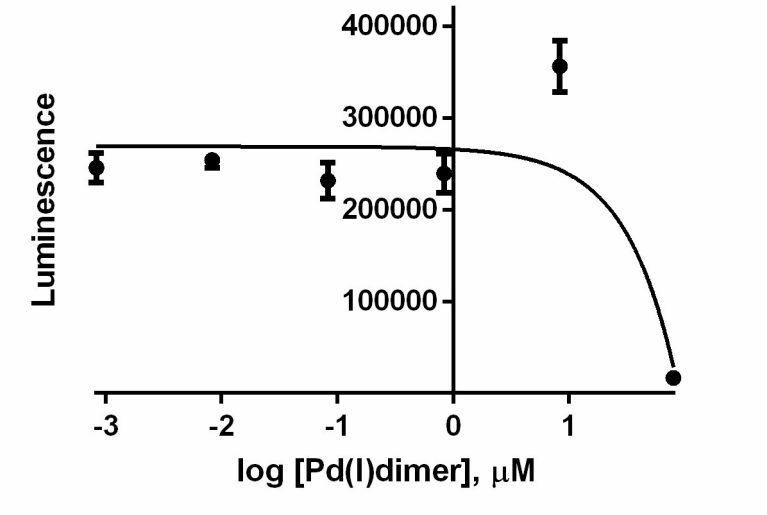

Figure S34: IC_{50} graph of MRC-5 cell line treated with Pd(I) dimer **3**.

References:

1. P. R. Auburn, P. B. Mackenzie and B. Bosnich, *J. Am. Chem. Soc.*, 1985, **107**, 2033–2046.
2. L. Canovese, F. Visentin, P. Uguagliati, G. Chessa and A. Pesce, *J. Organomet. Chem*., 1998, **566**, 61-71.
3. S. N. Sluijter, S. Warsink, M. Lutzc, C. J. Elsevier, *Dalton Trans.*, 2013, **42**, 7365-7372.
4. Scattolin, E. Bortolamiol, I. Caligiuri, F. Rizzolio, N. Demitri and F. Visentin, *Polyhedron*, 2020, **186**, 114607.
5. A. Lausi, M. Polentarutti, S. Onesti, J. R. Plaisier, E. Busetto, G. Bais, L. Barba, A. Cassetta, G. Campi, D. Lamba, A. Pifferi, S. C. Mande, D. D. Sarma, S. M. Sharma and G. Paolucci, *Eur. Phys. J. Plus*, 2015, **130(43)**, 1-8.
6. W. Kabsch, *Acta Crystallogr. D*, 2010, **66(2)**, 125-132.
7. G. M. Sheldrick, *Acta Crystallogr. A*, 2015, **71**, 3-8.
8. G. M. Sheldrick, *Acta Crystallogr. C*, 2015, **71**, 3-8.
9. P. Emsley, B. Lohkamp, W. Scott, K. Cowtan, *Acta Crystallogr. D*, 2010, **66**, 486-501.
10. L. Farrugia, *J. Appl. Cryst.*, 2012, **45(4)**, 849-851.
11. L. Schrodinger, *The PyMOL Molecular Graphics System*, 2015, http://www.pymol.org.
12. P. D. W. Boyd, A. J. Edwards, M. G. Gardiner, C. C. Ho, M. Lemée-Cailleau, D. S. McGuinness, A. Riapanitra, J. W. Steed, D. N. Stringer and B. F. Yates, *Angew. Chem. Int. Ed.*, 2010, **49**, 6315-6318.
13. D. P. Hruszkewycz, L. M. Guard, D. Balcells, N. Feldman, N. Hazari and M. Tilset, *Organometallics*, 2015, **34**, 381-394.
14. W. Dai, M. J. Chalkley, G. W. Brudvig, N. Hazari, P. K. R. Melvin, R. Pokhrel and M. K. Takase, *Organometallics*, 2013, **32**, 5114-5127.
15. P. Ai, C. Gourlaouen, A. A. Danopoulos and P. Braunstein, *Inorg. Chem.*, 2016, **55**, 1219-1229.
16. Gaussian 09, Revision D.01, M. J. Frisch, G. W. Trucks, H. B. Schlegel, G. E. Scuseria, M. A. Robb, J. R. Cheeseman, G. Scalmani, V. Barone, B. Mennucci, G. A. Petersson, H. Nakatsuji, M. Caricato, X. Li, H. P. Hratchian, A. F. Izmaylov, J. Bloino, G. Zheng, J. L. Sonnenberg, M. Hada, M. Ehara, K. Toyota, R. Fukuda, J. Hasegawa, M. Ishida, T. Nakajima, Y. Honda, O. Kitao, H. Nakai, T. Vreven, J. A. Montgomery, Jr., J. E. Peralta, F. Ogliaro, M. Bearpark, J. J. Heyd, E. Brothers, K. N. Kudin, V. N. Staroverov, T. Keith, R. Kobayashi, J. Normand, K. Raghavachari, A. Rendell, J. C. Burant, S. S. Iyengar, J. Tomasi, M. Cossi, N. Rega, J. M.

Millam, M. Klene, J. E. Knox, J. B. Cross, V. Bakken, C. Adamo, J. Jaramillo, R. Gomperts, R. E. Stratmann, O. Yazyev, A. J. Austin, R. Cammi, C. Pomelli, J. W. Ochterski, R. L. Martin, K. Morokuma, V. G. Zakrzewski, G. A. Voth, P. Salvador, J. J. Dannenberg, S. Dapprich, A. D. Daniels, O. Farkas, J. B. Foresman, J. V. Ortiz, J. Cioslowski, and D. J. Fox, Gaussian, Inc., Wallingford CT, 2013.

17. C. Adamo and V. Barone, *J. Chem. Phys.*, 1999, **110**, 6158−6170.
18. S. Grimme, J. Antony, S. Ehrlich and H. Krieg, *J. Chem. Phys.*, 2010, **132**, 154104−154119.
19. A. Schaefer, H. Horn and R. Ahlrichs, *J. Chem. Phys.*, 1992, **97**, 2571−2577.
20. (a) U. Haeusermann, M. Dolg, H. Stoll and H. Preuss, *Mol. Phys.*, 1993, **78**, 1211–1224; (b) W. Kuechle, M. Dolg, H. Stoll and H. Preuss, *J. Chem. Phys.*, 1994, **100**, 7535–7542; (c) T. Leininger, Nicklass, H. Stoll, M. Dolg and P. Schwerdtfeger, *J. Chem. Phys.*, 1996, **105**, 1052–1059.
21. A. V. Marenich, C. J. Cramer and D. G. Truhlar, *J. Phys. Chem. B*, 2009, **113**, 6378-6396.
22. A. Adan, Y. Kiraz and Y. Baran, *Curr. Pharm. Biotechnol.*, 2016, **17(14)**, 1213-1221.
23. H. Miyoshi and T. S. Stappenbeck, *Nat. Protoc.*, 2013, **8(12)**, 2471-2482.